

Cosmological constraints on sterile neutrino Dark Matter production mechanisms

Lucia Aurelia Popa

Institute of Space Science,
Bucharest-Magurele, Ro-077125 Romania

E-mail: lpopa@spacescience.ro

Abstract. We place constraints on sterile neutrino resonant production (RP) and scalar decay production (SDP) mechanisms assuming that sterile neutrino represents a fraction f_S from the total Cold Dark Matter energy density.

For the cosmological analysis, we complement the CMB anisotropies measurements with CMB lensing gravitational potential measurements, that are sensitive to the DM distribution out to high redshifts and with the cosmic shear data, that constraints the gravitational potential at lower redshifts than CMB. We also use the most recent low-redshift BAO measurements that are insensitive to the non-linear effects, providing robust geometrical tests.

We show that our datasets have enough sensitivity to constrain the sterile neutrino mass and mass fraction inside the co-moving free-streaming horizon in both RP and SDP scenarios.

For RP case we find that the best fit values of sterile neutrino mass and mixing angle are in the parameter space of interest for sterile neutrino DM decay interpretation of the 3.5 keV X-ray line with a DM mass fraction $f_S = 0.28 \pm 0.3$ (at 68% CL) that excludes the assumption of sterile neutrinos as being all of the DM. For SDP case we find $f_S = 0.86 \pm 0.07$ (at 68% CL), in agreement with the upper limit constraint on f_S from the X-ray non-detection and Ly- α forest measurements that rejects $f_S = 1$ at 3σ level [1].

The sterile neutrino mass predicted by both RP and SDP models are consistent within 0.3σ . We analysed the possibility to distinguish between RP and SDP scenarios through their impact on the acoustic scales, the small scale fluctuations and the low-redshift geometric observables, obtaining cosmological constraints that clearly show that the present-day cosmological data start to discriminate between different sterile neutrino DM production mechanisms.

However, we expect the future BAO and weak lensing surveys, such as EUCLID, to provide much robust constraints.

Keywords: cosmic microwave background, dark matter, dark energy, cosmological observations

Contents

1	Introduction	1
2	Sterile neutrino DM production mechanisms	3
2.1	Sterile neutrino resonant production (RP)	4
2.2	Sterile neutrino production by the scalar decay (SDP)	7
3	Parameterisation and methods	7
4	Cosmological data	10
5	Analysis and results	11
5.1	Sensitivity of cosmological data to sterile neutrino mass and mass fraction	11
5.2	Constraints on sterile neutrino DM production parameters	14
5.3	Cosmological predictions of sterile neutrino production mechanisms	15
5.3.1	Acoustic scales	15
5.3.2	Small-scale fluctuations	15
5.3.3	Low-redshift geometric probes	18
6	Conclusions	19

1 Introduction

Cosmic Microwave Background (CMB) measurements from the PLANCK satellite, alone or in combination with other astrophysical datasets, provide no powerful evidence supporting new physics beyond the standard Λ CDM cosmological model [2, 3, 4].

With around 5% of the total energy density of the universe representing the baryonic matter, 21% the Dark Matter (DM) and 74% accounting for the Dark Energy (DE), the Λ CDM model is remarkably successful at reproducing the large-scale structure (LSS) of the universe. In addition, the Planck results show that the signature of neutrino sector is consistent with the Λ CDM model assumptions and that DE is compatible with the Λ cosmological constant.

Some tension still exists between the PLANCK determination of several observables and their values obtained from astrophysical independent probes. The most notable tension concern the smaller value of the Hubble constant, H_0 , discordant at about 2.5σ level with the value obtained from direct astrophysical measurements [5, 6, 7]. Also, PLANCK determination of σ_8 (the amplitude of linear power spectrum on scale of $8h^{-1}$ Mpc, h being the reduced Hubble constant, $h = H_0/(100 \text{ km s}^{-1} \text{ Mpc}^{-1})$) and of matter energy density, Ω_m , are discordant at 2σ level with the corresponding values inferred from cluster data that prefer lower values of these observables [8, 9]. These discrepancies may arise because of biases and calibration errors of direct astrophysical measurements [3, 10] but may also be related to the assumption of the underlying Λ CDM cosmological model [11].

Interpretation of DE in the form of Λ is facing challenges such as the cosmological constant problem [12] and the coincidence problem [13]. The first problem refers to the small observed value of Λ , incompatible with the prediction of the field theory. The second problem regards the fact that there is not a natural explanation why DM and DE energy densities are of

the same order of magnitude today. Alternative DE models aiming to alleviate these problems have been proposed. In these models DE is generally described by a dynamical cosmological fluid associated either to a scalar field [14] or to modifications of gravity [15, 16], although a quantum running of Λ could provide a satisfactory evolving DE scenario [17, 18, 19].

The nature and composition of DM is still unknown. Attempts involving collision-less DM particles fail to solve the Λ CDM problems at reproducing the cosmological structures at small scales (missing satellite problem [20, 21, 22], core-cusp problem [23, 24, 25], too-big-to-fail problem [26, 27]), suggesting that DM particles may also exhibit gravitational properties and requiring the extension of the Standard Model (SM) of particle physics [28, 29, 30].

The Weakly Interacting Massive Particles (WIMPs) with masses above the electroweak scale are good DM candidates [31]. As WIMPs decouple from the thermal plasma when the Hubble expansion rate becomes larger than their interaction rate (thermal *freeze-out*). Although well theoretically motivated, currently no conclusive WIMPs experimental evidences have been found (see e.g. [32] and references therein).

Another theoretically well motivated DM candidate is sterile neutrino [33, 34, 35, 36]. Arising in the minimal extension of SM, the sterile neutrino with mass in keV range can simultaneously explain the active neutrino oscillations, the DM properties and the matter-antimatter asymmetry of the universe [37, 38]. Detection of a weak X-ray emission line at an energy of ~ 3.5 keV from clusters and Andromeda galaxy independently reported by XMM-Newton and Chandra satellites [39, 40] initiated a large debate on the possibility that this line is the signature of DM decay [41, 42, 43]. If confirmed, this signal could be the signature of decaying sterile neutrino DM with a mass of 7.1 keV [44].

As sterile neutrinos are weakly interacting particles they cannot be produced in the early universe by *thermal freeze-out*. Instead they could be gradually produced from the thermal plasma by the *thermal freeze-in* [45] with non-thermal spectrum, the dominant production occurring when the temperature drops below the sterile neutrino mass. Several keV sterile neutrino DM production mechanisms have been proposed.

In the Dodelson-Widrow (DW) scenario [46], keV sterile neutrinos DM are produced by non-resonant oscillations with active neutrinos in presence of negligible leptonic asymmetry. This mechanism is now excluded by the observations of structure formation as it produces too hot sterile neutrino velocity spectra [47, 48].

The keV sterile neutrino DM resonant production (RP) via the conversion of active to sterile neutrinos through Shi-Fuller mechanism [49] in presence of leptonic asymmetry has also been investigated [50, 51, 52]. In this scenario, sterile neutrino parameters required to reproduce the X-ray line of ~ 3.5 keV are consistent with main cosmological parameters inferred from present cosmological measurements, Local Group and high- z galaxy count constraints and successfully solve the missing satellite and too-big-to-fail problems [53, 54, 81]. Some tension with Ly- α data still exists (at 2.5σ level) [55]. This tension however, which could be related to some uncertainties in theoretical modelling of the intergalactic medium (IGM) and the associated numerical methods [56, 81], is not strong enough to rule out the RP scenario.

The keV sterile neutrino DM production by particle decays has been also extensively discussed [57, 58, 59, 60, 61]. A particularly interesting case is the DM sterile neutrino production by scalar decay (SDP). This process involves a generic scalar singlet with the vacuum expectation value (vev) $\langle S \rangle$ that could be produced via SM Higgs interactions. Depending on the strength of the Higgs coupling λ_H , the singlet scalar can be produced like WIMPs via *freeze-out* [62, 63, 64] or like “Feeble Interacting Massive Particles” (FIMPs) via *freeze-in* [55, 66] mechanisms and must couple with the right-handed neutrino fields through Yukawa interac-

tion, leading to sterile neutrino Majorana masses $m_N = y_k \langle S \rangle$, where y_k is the Yukawa coupling strength. Ref. [67] presents a complete treatment of the SDP mechanism for the whole parameter space, giving the general solution on the level of momentum distribution function.

Other proposed mechanisms are the production via interactions with the inflaton field [69, 70], or production from pion decays [71].

The coupled DE models (CDE) in which the DM particles, in addition to the gravitational interaction, have an interaction mediated by the DE scalar field have been also studied. A classification of these models can be found in Ref. [16]. The strength of coupling modifies the shape and amplitude of cosmological perturbations [72], affecting the growth rate of cosmological structures [73]. Moreover, the strength of the coupling is degenerate with the amount of DM energy density, with impact on different cosmological parameters, including the Hubble expansion rate [74] and equation of state of DE [75].

So far, the keV sterile neutrino DM properties have been addressed by evaluating their impact on the co-moving free streaming horizon, that relates on the average velocity distribution. However, for such models characterised by a highly non-thermal momentum distribution, the average momentum is subject of uncertainties, leading to a fail of free-streaming horizon in constraining the sterile neutrino parameters [65]. The existing constraints are in general obtained in linear theory under the assumption that sterile neutrinos are all of the DM [66, 76, 77].

The aim of this paper is to place constraints on RP and SDP mechanisms through their impact on distance-redshift relations and the growth of structures. We consider models where DM is a mixture of CDM and sterile neutrino produced via RP and SDP mechanisms and analyse if this mixture can be compensated by changes in cosmological parameters.

We use the existing measurements of the CMB gravitational potential, of the baryon acoustic oscillation (BAO) and of the weak gravitational lensing of galaxies to discriminate between different sterile neutrino DM production mechanism through the impact on the acoustic scales, the small scale fluctuations and the low-redshift probes.

The paper is organised as follows: Section 2 summarise the RP and SDP Boltzmann formalisms calculations. Section 3 describes the model parameters and the methods involved in the analysis. Section 4 presents the datasets. Section 5 presents our results and examine the consistency and cosmological implications of sterile neutrino DM production mechanisms. The conclusions are summarised in Section 6.

2 Sterile neutrino DM production mechanisms

In this section we present the sterile neutrino DM production calculations. We compute the evolution of phase space distributions in an homogeneous and isotropic Friedman-Robertson-Walker universe employing the Boltzmann equation:

$$\hat{L}[f] = \mathcal{C}[f], \quad (2.1)$$

where f is the phase space distribution, \mathcal{C} is the collision term which encodes the details of a specific sterile neutrino DM production mechanism and \hat{L} is the Liouville operator:

$$\hat{L} = \frac{\partial}{\partial t} - \mathcal{H}p \frac{\partial}{\partial p}, \quad (2.2)$$

where p is the particle momentum and \mathcal{H} is the Hubble function. In order to bring Eq. (2.2) into a more convenient form, we perform the following transformation of variables [67]:

$$\begin{aligned} t &\rightarrow r = r(t, p), \\ p &\rightarrow \xi = \xi(t, p). \end{aligned} \quad (2.3)$$

Exploiting the correspondence between temperature T and time t and by using the conservation of the comoving entropy, the above transformations can be written in the form (for details see Appendix A.2 from Ref. [67]):

$$\begin{aligned} r &= \frac{m_0}{T}, \\ \xi &= \left(\frac{g_s(T_0)}{g_s(T)} \right)^{1/3} q, \end{aligned} \quad (2.4)$$

where $q = p/T$ is the co-moving momentum and $g_s(T)$ is the effective number of relativistic entropy degrees of freedom. We choose $m_0 = T_0 = m_h$ where $m_h = 125$ GeV is the Higgs boson mass. In terms of the variables given in Eqs.(2.4), the Liouville operator reads as:

$$\hat{L} = \mathcal{H}r \left(\frac{Tg'_s(T)}{3g_s(T)} + 1 \right)^{-1} \frac{\partial}{\partial r}, \quad (2.5)$$

and the time-temperature relation is given by:

$$\frac{dT}{dt} = -\mathcal{H}T \left(\frac{Tg'_s(T)}{3g_s(T)} + 1 \right)^{-1}, \quad (2.6)$$

where $'$ denotes the derivative with respect to the temperature T . We used the fitting formulas from Ref.[78] to compute the temperature evolution of the effective number of relativistic entropy degrees of freedom $g_s(T)$ and its derivative $g'_s(T)$.

2.1 Sterile neutrino resonant production (RP)

The Boltzmann equation describing the sterile neutrino RP in terms of variables given by Eqs. (2.4) can be written as:

$$\mathcal{H}r \left(\frac{Tg'_s(T)}{3g_s(T)} + 1 \right)^{-1} \frac{\partial}{\partial r} f_{\nu_s}(r, \xi) \simeq \Gamma(f_{\nu_\alpha} \rightarrow f_{\nu_s}) [f_{\nu_\alpha}(r, \xi) - f_{\nu_s}(r, \xi)]. \quad (2.7)$$

There is similar equation for antineutrinos $\bar{\nu}_\alpha$. In the above equation f_{ν_α} ($\alpha = e, \mu, \tau$) is the active neutrino momentum distribution function, f_{ν_s} is the sterile neutrino momentum distribution function and $\Gamma(\nu_\alpha \rightarrow \nu_s)$ is the sterile neutrino effective production rate [34, 50].

$$\Gamma(\nu_\alpha \rightarrow \nu_s) \approx \frac{1}{4} \Gamma_{\nu_\alpha}(p, T) \sin^2 2\theta_M, \quad (2.8)$$

where Γ_{ν_α} is the collision rate and θ_M is the effective matter mixing angle:

$$\sin^2 2\theta_M = \frac{\Delta^2(p) \sin^2 2\theta}{\Delta^2(p) \sin^2 2\theta + D^2(p) + [\Delta(p) \cos 2\theta + V^L - V^T]^2}. \quad (2.9)$$

Here θ is the vacuum mixing angle, $\Delta(p) = \delta m^2/2p$ is the vacuum oscillation factor, $D(p) = \Gamma_{\nu_\alpha}(p)/2$ is the quantum damping rate, V^T is the thermal potential and V^L is the asymmetric lepton potential. For temperatures characteristic to the post weak decoupling era ($T < 3$ MeV), the contribution of the thermal potential is very small and can be neglected. In the presence of a primordial lepton asymmetry V^L is given by:

$$V^L = 2\sqrt{2}\zeta_R(3)\pi^{-2}G_F T^3 \mathcal{L}_\alpha. \quad (2.10)$$

where G_F is the Fermi constant, $\zeta_R(3)$ is the Reimann function of 3 and \mathcal{L}_{ν_α} is the potential lepton number corresponding to the active neutrino flavour α :

$$\mathcal{L}_{\nu_\alpha} \equiv 2L_{\nu_\alpha} + \sum_{\beta \neq \alpha} L_{\nu_\beta}, \quad L_{\nu_\beta} = \left(\frac{1}{12\zeta_R(3)}\right) \left(\frac{T_\nu}{T_\gamma}\right)^3 [\pi^2 \zeta_{\nu_\alpha} + \zeta_{\nu_\alpha}] \quad \beta = (e, \mu, \tau) \quad (2.11)$$

In the above equation $\pm\zeta_{\nu_\alpha}$ is $\nu_\alpha/\bar{\nu}_\alpha$ chemical potential, L_{ν_β} is the lepton number and T_ν is the present temperature of the neutrino background [$T_\nu/T_\gamma = (4/11)^{1/3}$]. The MSW condition for the resonant scaled neutrino momentum ζ_{res} is given by:

$$\zeta_{res} = \left(\frac{g_s(T_0)}{g_s(T)}\right)^{1/3} \left(\frac{p}{T}\right)_{res} \approx \left(\frac{\delta m^2 \cos 2\theta}{4\sqrt{2}\zeta_R(3)\pi^{-2}G_F \mathcal{L}_{\nu_\alpha}}\right) T^{-4}, \quad (2.12)$$

where $\delta m^2 = m_2^2 - m_1^2 \approx m_2^2$ is the difference of the squares of sterile neutrino and active neutrino mass eigenvalues, T is the plasma temperature and θ is the vacuum mixing angle. The evolution of the potential lepton number when the resonant active neutrino momentum sweeps from 0 to ζ_{res} is then given by:

$$\mathcal{L}_{\nu_\alpha}(\zeta_{res}) = \mathcal{L}^{init} - \frac{1}{2\zeta_R(3)} \left(\frac{T_\nu}{T_\gamma}\right)^3 \int_0^{\zeta_{res}} (1 - e^{-\pi\gamma/2}) f_{\nu_\alpha} d\zeta, \quad (2.13)$$

where f_{ν_α} is the initial neutrino Fermi-Dirac momentum distribution and γ is the dimensionless adiabaticity parameter [79]. The sterile neutrino number density $n_{\nu_s}(r)$ and the sterile neutrino physical energy density $\Omega_{\nu_s} h^2$ are then given by:

$$n_{\nu_s}(r) = \frac{N}{2\pi^2} \frac{g_s(T)}{g_s(T_0)} \left(\frac{m_0}{r}\right)^3 \int_0^\xi d\xi \xi^2 f_{\nu_s}(\xi, r), \quad (2.14)$$

$$\Omega_{\nu_s} h^2 = \frac{s_0}{s(r)} \frac{m_{\nu_s} n_{\nu_s}(r)}{\rho_c/h^2}, \quad (2.15)$$

where $s(r)$ is the co-moving entropy density, $s_0=2891.2 \text{ cm}^{-3}$ is the entropy density at the present time and $\rho_c/h^2=1.054 \cdot 10^{-2} \text{ MeV cm}^{-3}$ is the critical density in terms of reduced Hubble constant h .

The sterile neutrino RP mechanism is parameterised with respect to the sterile neutrino mass m_{ν_s} , the matter mixing angle $\sin^2 2\theta$, and the initial lepton asymmetry of each active neutrino flavour, \mathcal{L}_{ν_α} . We simultaneously evolve Eqs. (2.6), (2.7), (2.12) and (2.13) to obtain the active and sterile neutrino phase-space distributions in the expanding universe for the entire range of resonant scaled neutrino momentum. The details of this computation can be found in Ref. [80]. Fig. 1 presents in the left panel the dependence of the sterile neutrino final

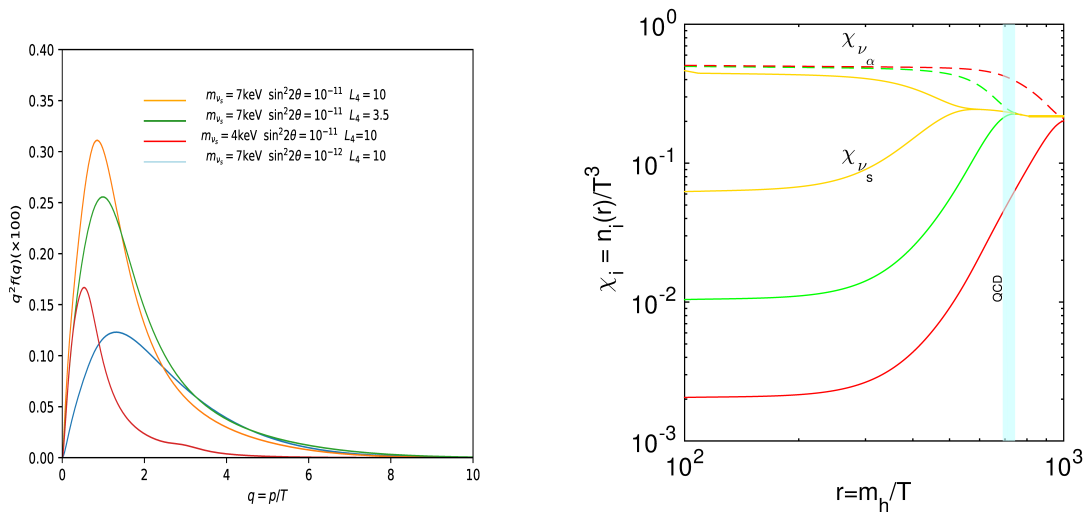


Figure 1: *Left:* The dependence of the sterile neutrino final momentum distributions on the co-moving momentum $q = p/T$ for different values of m_{ν_s} , $\sin^2 2\theta$ and $L_4 = 10^4 \times L_\nu$. *Right:* The dependence of the abundances of sterile neutrino (continuous lines) and active neutrino (dashed lines) on the time parameter $r = m_h/T$ for the same models presented in the left panel. The vertical light blue line indicates the temperature of the QCD phase transition ($T_{QCD} = 173 \pm 8\text{MeV}$ [81]). Other parameters are fixed to: $\Omega_b h^2 = 0.0226$, $\Omega_c h^2 = 0.112$, $\Omega_\nu h^2 = 0.00064$, $H_0 = 70 \text{ km s}^{-1} \text{ Mpc}^{-1}$ and $\Omega_K = 0$.

momentum distributions on the co-moving momentum $q = p/T$ for different values of m_s , $\sin^2 2\theta$ and \mathcal{L}_{ν_α} . The effect of increasing \mathcal{L}_{ν_α} when m_s and $\sin^2 2\theta$ are fixed is the increase of the averaged co-moving momentum, leading to a larger cutoff scales in the gravitational potential and matter power spectra. The same behaviour is present when $\sin^2 2\theta$ and \mathcal{L}_{ν_α} are fixed and m_s is increased. A larger value of $\sin^2 2\theta$ leads to larger sterile neutrino production rates. The resonance occurs in this case at a higher temperature and smaller averaged co-moving momentum. The same behaviours are shown by these models in the right panel from Fig. 1 that presents the evolution with time parameter $r = m_h/T$ of active and sterile neutrino abundances $\chi(r) = n(r)/T^3$, where $n(r)$ are corresponding number densities.

There are few shortcomings related to this computation. The calculation of sterile neutrino momentum distribution is based on the semi-classical Boltzmann formalism which is accurate only if the collisions dominate the neutrino interactions. This restricts the sterile neutrino parameter space to $\Delta(p) \sin^2 2\theta / D(p) < 1$ [82], which we took into account in the cosmological analysis. Our computation is also restricted to the mixing of ν_s with one active flavour $\nu_\mu / \bar{\nu}_\mu$, ignoring the mixing with other flavours that may have similar momentum distributions [83]. We also assume the same initial lepton asymmetry of each $\nu / \bar{\nu}$ flavour and ignore the redistribution of the lepton asymmetry during the QCD phase-transition and the opacities of active neutrinos. However, in Ref. [82] it is shown that these approximations do not significantly affect the sterile neutrino momentum distribution.

We used the sterile neutrino production code `sterile-dm` from [82], that includes the initial lepton asymmetry redistribution and neutrino opacity correction, to test our production code. We find a good agreement between the momentum distributions. We then implement the momentum distributions obtained with `sterile-dm` code in our production code and find

$\Omega_{\nu_s} h^2$ in agreement up to $\pm 5\%$, for a large range of parameter space. We also find that the sterile neutrino momentum distributions obtained with our code are in agreement with the similar momentum distributions presented in Refs. [77, 84].

2.2 Sterile neutrino production by the scalar decay (SDP)

In the case of SDP mechanism, the evolution of momentum distributions for scalar, f_S , and sterile neutrino, f_{ν_s} , are obtained by solving the coupled Boltzmann equations:

$$\hat{L}[f_S] = \mathcal{C}^S, \quad \hat{L}[f_{\nu_s}] = \mathcal{C}^{\nu_s}, \quad (2.16)$$

where \hat{L} is the Liouville operator given in Eq. (2.5) and \mathcal{C}^S and \mathcal{C}^{ν_s} are the scalar and sterile neutrino collision terms encoding the effects of different processes that contribute to their production. In this work we take the leading processes contributing to \mathcal{C}^S and \mathcal{C}^{ν_s} :

$$\begin{aligned} \mathcal{C}^S &= \mathcal{C}_{hh \leftrightarrow SS}^S + \mathcal{C}_{S \rightarrow \nu_s \nu_s} \\ \mathcal{C}^{\nu_s} &= \mathcal{C}_{S \rightarrow \nu_s \nu_s}^{\nu_s} \end{aligned} \quad (2.17)$$

where: $\mathcal{C}_{hh \leftrightarrow SS}^S$ describes the depletion of scalars due to the annihilation into pairs of SM Higgs particles and the reverse process, $\mathcal{C}_{S \rightarrow \nu_s \nu_s}$ describes the decay of scalars into pairs of sterile neutrinos and $\mathcal{C}_{S \rightarrow \nu_s \nu_s}^{\nu_s}$ describes the creation of sterile neutrinos from the decays of scalars. A detailed discussion regarding the contributions of different processes to the collision terms can be found in Refs. [66, 67].

With these assumptions, the SDP scenario is parametrised with respect to the sterile neutrino mass m_{ν_s} , the scalar mass M_S , the strength of the Higgs coupling λ_H and of the Yukawa coupling y_k . We use the explicit forms of the collision terms given in Ref. [67] and simultaneously evolve Eqs. (2.6) and (2.16) to obtain the scalar and sterile neutrino momentum distributions in the expanding universe. The sterile neutrino number density and the corresponding physical energy density are then obtained by using Eqs. (2.14) and (2.15). Left panel from Fig. 2 presents the dependence of the sterile neutrino final momentum distribution on the co-moving momentum $q = p/T$ for different values of λ_H and y_k . The right panel shows the evolution with time parameter $r = m_h/T$ of scalar and sterile neutrino abundances $\chi(r) = n(r)/T^3$. The distributions obtained for the best fit parameters are also presented by.

We neglect in our computation the mixing between active and sterile neutrino and therefore the contribution of DW mechanism, shown to have a very small contribution to the sterile neutrino production [68]. We test the production code over a large parameter space and find that our distributions are in agreement with the similar distributions presented in Refs. [66, 67].

3 Parameterisation and methods

The baseline model is an extension of the flat Λ CDM model, described by the following cosmological parameters:

$$\mathbf{P}_{\Lambda\text{CDM}} = \left\{ \Omega_b h^2, \Omega_c h^2, \theta_s, \tau, \log(10^{10} A_s), n_s, \sum m_\nu, N_{eff} \right\},$$

where: $\Omega_b h^2$ is the present baryon energy density, $\Omega_c h^2$ is present CDM energy density, θ_{MC} the ratio of sound horizon to angular diameter distance at decoupling, τ is the optical depth at reionization, A_s and n_s are amplitude and spectral index of primordial power spectrum of

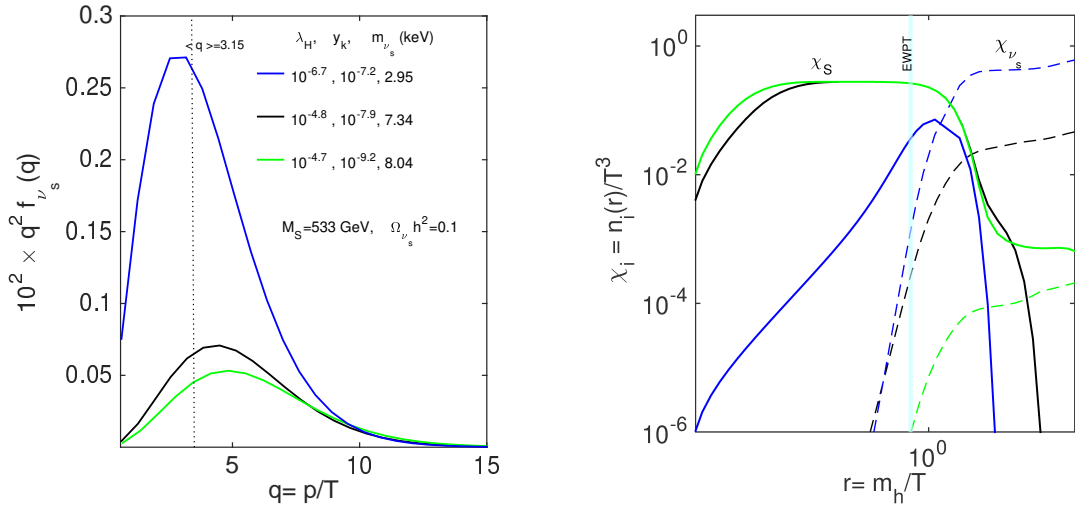


Figure 2: *Left:* The dependence of the sterile neutrino final momentum distributions on the co-moving momentum $q = p/T$ for scalar mass $M_S=533$ GeV (the best fit value) and different values of the Higgs coupling, λ_H , and Yukawa coupling, y_k . The dotted line indicates the value of the averaged co-moving momentum corresponding to sterile neutrino thermally produced. *Right:* The dependence of the abundances of scalar (continuous lines) and sterile neutrino (dashed lines) on the time parameter $r = m_h/T$ for the same models presented in the left panel. The vertical blue line indicates the temperature of the electroweak phase transition. The distributions corresponding to the best fit parameters from our cosmological analysis are presented in both panels (black lines). Other parameters are fixed to: $\Omega_b h^2 = 0.0226$, $\Omega_c h^2 = 0.112$, $\Omega_\nu h^2 = 0.00064$, $H_0=70$ km s $^{-1}$ Mpc $^{-1}$ and $\Omega_K = 0$.

curvature perturbations at pivot scale $k = 0.05$ Mpc $^{-1}$, $\sum m_\nu$ is the total mass of three active neutrino flavours and N_{eff} the number of relativistic degrees of freedom that parametrise the contributions from any non-interacting relativistic particles. In the SM with three active neutrino flavours, $N_{eff}=3.046$ due to non-instantaneous decoupling corrections [85].

The *RP mechanism model* includes, in addition to the baseline model parameters, the following parameters:

$$\mathbf{P}_{RP} = \{ \zeta_\nu, m_{\nu_s}, \sin^2 2\theta \},$$

where: $\pm\zeta_\nu$ is the total chemical potential of three degenerated active $\nu/\bar{\nu}$ species, m_{ν_s} is the sterile neutrino mass and $\sin^2 2\theta$ is the mixing angle.

The *SDP mechanism model* extend the baseline model by including the following parameters:

$$\mathbf{P}_{SDP} = \{ m_{\nu_s}, M_S, y_k, \lambda_H \},$$

where: m_{ν_s} is the sterile neutrino mass, M_S is the scalar mass, y_k is the Yukawa strengths coupling and λ_H the Higgs strengths coupling.

The sterile neutrino mass fraction is a derived parameter, $f_S = \Omega_{\nu_s}/\Omega_c$, where the sterile neutrino energy density Ω_{ν_s} is computed by using Eq. (2.15). The matter energy density in RP and SDP scenarios is then given by $\Omega_m = \Omega_c + \Omega_b + \Omega_\nu + \Omega_{\nu_s}$.

We modify the baseline Boltzmann code `camb`¹ [86] to allow the calculation of sterile neutrino DM production formalisms presented in the previous section.

Non-linear corrections: We use the `halofit` model [87, 88] implemented in the `camb` code to account for the non-linear effects in CMB anisotropy and lensing potential power spectra.

Recombination: The process of recombination determines the size of the sound horizon at this epoch, affecting the characteristic angular size of the CMB fluctuations and the diffusion damping scale. We use the recombination model developed in Ref. [89] and further improved for full numerical implementation in the `recfast`² code [90].

Nucleosynthesis: The model of the Big Bang Nucleosynthesis (BBN) gives the relation between helium mass fraction, Y_P , photon-to-baryon ratio, ρ_γ/ρ_b , and the number of relativistic degrees of freedom, N_{eff} . In the case of RP mechanism, the leptonic asymmetry increases the radiation energy density parametrised by variation of the number of relativistic degrees of freedom ΔN_{eff} :

$$\Delta N_{eff}(\zeta_\nu) = 3 \left[\frac{30}{7} \left(\frac{\zeta_\nu}{\pi} \right)^2 + \frac{15}{7} \left(\frac{\zeta_\nu}{\pi} \right)^4 \right]. \quad (3.1)$$

The leptonic asymmetry also shifts the beta equilibrium between protons and neutrons with effects on Y_P that decreases with the increase of ζ_ν . The electron neutrino/antineutrino, $\nu_e/\bar{\nu}_e$, phase-space distributions determine the rates of the neutron and proton interaction at BBN. In the RP model, the non-thermal $\nu_e/\bar{\nu}_e$ spectra change these rates and hence the Y_P value over the case with thermal Fermi-Dirac spectrum [91, 92]. We use the PArthENoPE BBN code [93] to set the value of Y_P . For SDP model we compute the dependence of Y_P on $\Omega_b h^2$ and N_{eff} . For the RP model we consider in addition the effects on Y_P and ζ_ν for the change of neutron and proton interaction rates.

The parameter extraction from cosmological datasets is based on Monte-Carlo Markov Chain (MCMC) technique. We modify the latest publicly available version of the package `CosmoMC`³ [94] to sample from the space of cosmological and sterile neutrino production mechanism parameters and generate estimates of their posterior mean and confidence intervals. We first run the modified versions of `CosmoMC` and `camb` setting to zero the additional parameters for RP and SDP models. In both cases we find good consistency between our bounds and the existing constraints for Λ CDM model [3]. We use the default convergence settings implemented in `CosmoMC`: `MPLLimit_Converge` = 0.025 and `MPLLimit_Converge_Err` = 0.2. With these choices the `CosmoMC` run stops when the confidence interval for each parameter at 95% C.L. is accurate at 0.2σ . This error can be reduced, but in this case the computing time increases to reach the convergence limit. This become critical for non-standard models, as RP and SDP, for which the execution time is larger than in the standard case because of numerical evolution of momentum distributions in `camb`.

We use the same convergence criteria and made few test runs for RP and SDP models to optimise the prior intervals and sampling. The final runs are based on 120 independent channels for each model, reaching the convergence criterion $(R-1) \simeq 0.01$ for RP model and $(R-1) = 0.007$ for SDP model. The $(R-1)$ criterion is defined as the ratio between the variance of the means and the mean of variances for the second half of chains [94].

We assume a flat Universe and uniform priors for all parameters adopted in the analysis in the intervals listed in Tab. 1 and Tab. 2. The Hubble expansion rate H_0 and sterile

¹<http://camb.info>

²<http://www.astro.ubc.ca/people/scott/recfast.html>

³<http://cosmologist.info/cosmomc/>

Table 1: Priors and constraints for the Λ CDM-ext parameters adopted in the analysis. All priors are uniform in the listed intervals. We assume a flat Universe.

Parameter	Prior
$\Omega_b h^2$	[0.005, 0.1]
$\Omega_c h^2$	[0.001, 0.5]
$100\theta_s$	[0.5, 10]
τ	[0.01, 0.9]
$\log(10^{10} A_s)$	[2.5, 5]
n_s	[0.5, 1.5]
m_ν (eV)	[0, 6]
N_{eff}	[3.046, 8]
H_0 (km s $^{-1}$ Mpc $^{-1}$)	[20, 100]

Table 2: Priors and constraints on the additional parameters for RP and SDP models. All priors are uniform in the listed intervals.

RP Parameter	Prior	SDP Parameter	Prior
m_{ν_s} (keV)	[2, 30]	m_{ν_s} (keV)	[2, 30]
$10^{10} \times \sin^2 2\theta$	[0.1, 100]	y_k	[10^{-10} , 10^{-8}]
ζ_ν	[-0.1, 0.1]	λ_H	[10^{-8} , 10^{-4}]
		M_S (GeV)	[10, 1000]
$\Omega_{\nu_s} h^2$	[0.001, 0.5]	$\Omega_{\nu_s} h^2$	[0.001, 0.5]

neutrino energy density $\Omega_{\nu_s} h^2$ are derived parameters in our analysis. We constrained H_0 values to reject the extreme models and restrict the values of $\Omega_{\nu_s} h^2$ to the interval of $\Omega_c h^2$. The sterile neutrino mass lower limit is restricted by the Tremain-Gunn bound [95] while the upper limit is restricted by the non-detection of emission lines from X-ray observations [96].

4 Cosmological data

For our cosmological analysis we use the following datasets:

The CMB measurements: We use the CMB angular power spectra from PLANCK 2015 release [97] and the PLANCK likelihood codes [98] corresponding to different multipole ranges: **Commander** for $2 \leq l \leq 29$, **CamSpec** $50 \leq l \leq 2500$, **LowLike** for $2 \leq l \leq 32$ for polarization data and **Lensing** for $40 \leq l \leq 400$ of lensing data. As sterile neutrino production is expected to affect the redshift - distance relations and the growth of structures, we include in the analysis the PLANCK power spectrum of the reconstructed lensing potential [99]. We will refer tot the combination of these measurements as PLANCK+lens dataset.

Baryonic acoustic oscillations (BAO): BAO measurements are low-redshift probes insensitive to non-linear effects because their characteristic acoustic scale, of around 147 Mpc, is much larger than the scale of the virialized cosmological structures. Moreover, as BAO

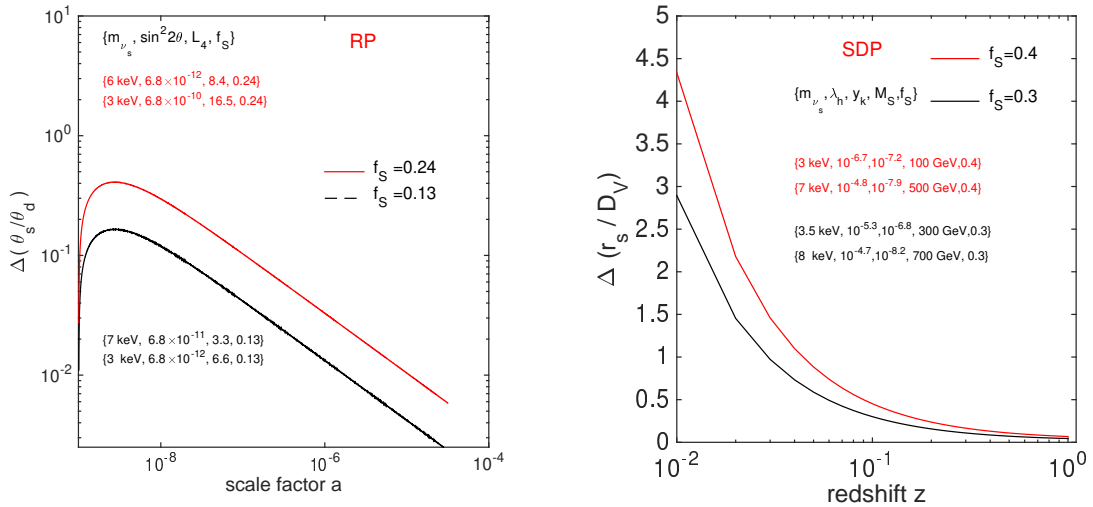


Figure 3: *Left:* The evolution to photon decoupling of the variation $\Delta(\theta_s/\theta_d)$ for models sharing the same sterile neutrino mass fraction f_S obtained in the RP scenario. *Right:* The redshift dependence of the variation of BAO characteristic parameter, $\Delta(r_s(z_d)/D_V(z))$, for models sharing the same sterile neutrino mass fraction f_S obtained in SDP scenario. The production mechanism parameters are indicated for each case. Other parameters are fixed to: $\Omega_b h^2 = 0.0226$, $\Omega_c h^2 = 0.112$, $\Omega_\nu h^2 = 0.00064$, $H_0 = 70 \text{ km s}^{-1} \text{ Mpc}^{-1}$ and $\Omega_K = 0$.

features in the matter power spectrum can be observed as a function of both angular and redshift separations [100, 101] these measurements are robust geometrical tests. We include in analysis the BAO characteristic parameter measurements from Baryon Oscillation Spectroscopic Survey (BOSS) LOWZ at $z_{eff} = 0.32$ and CMASS at $z_{eff} = 0.57$ [101], BOSS DR12 at $z_{eff} = 0.38, 0.51$ and 0.61 [102] and 6dF Galaxy Survey (6dFGS) at $z_{eff} = 0.1$ [103]. We will refer to the combination of these measurements as BAO dataset.

Cosmic shear: Weak lensing of galaxies, or cosmic shear, constraints the gravitational potential at redshifts lower than the CMB lensing. Presently, the cosmic shear measurements are available from several surveys [104, 105, 106]. We use the COSMOMC implementation of one-year Dark Energy Survey (DES) [107] cosmic shear measurements described in Ref. [108], referred hereafter as DES dataset.

5 Analysis and results

5.1 Sensitivity of cosmological data to sterile neutrino mass and mass fraction

A change in sterile neutrino mass fraction f_S leads first to a change in the Hubble expansion rate H . At the CMB photons decoupling ($T_{\text{cmb}} = 0.26 \text{ eV}$) this change the sound horizon distance r_s (that scales as $1/H$) and in the photon diffusion dumping distance r_d (that scales as $\sqrt{1/H}$). The CMB anisotropy spectrum is sensitive to both r_s and r_d changes as projected angles over the co-moving angular distance, D_A , to the last scattering: $\theta_s = r_s/D_A$ and $\theta_d = r_d/D_A$. While a change in θ_s shifts the position of the acoustic Doppler peaks through the CMB anisotropy spectrum, a change in θ_d relative to θ_s modify its amplitude. CMB can measure the expansion rate by measuring the ratio $\theta_d/\theta_s \sim \sqrt{H}$.

For models sharing the same value of f_S , the ratio θ_d/θ_s is a measure of the relativistic energy density at T_{cmb} , usually parametrised by $N_{\text{eff}}(T_{\text{cmb}})$ [109]. The contribution of sterile neutrinos to $N_{\text{eff}}(T_{\text{cmb}})$ encodes information on their mass and production mechanism parameters that lies in the momentum distribution function and can be computed by comparing the sterile neutrino kinetic energy density to the energy density of other relativistic particles in equilibrium at T_{cmb} [66]. This contribution is very small in the case of sterile neutrinos produced via SDP mechanism since in this case sterile neutrinos cooled down at T_{cmb} and have smaller co-moving momenta when comparing to the RP mechanism.

Left panel from Fig. 3 presents the evolution to photon decoupling of the variation $\Delta(\theta_s/\theta_d)$ obtained in RP case for models sharing the same sterile neutrino mass fraction. The figure shows that an accurate determination of θ_s/θ_d breaks the degeneracy of Hubble parameter at T_{cmb} , leading to constraints on sterile neutrino mass and production parameters.

The BAO measurements lead to joint constraints on the co-moving angular diameter distance, $D_A(z)$, and the Hubble parameter, $H(z)$, at smaller redshifts than CMB. At these redshifts, for models sharing the same sterile neutrino mass fraction, both $D_A(z)$ and $H(z)$ are degenerated. The BAO observations typically constrain the quantity $r_s(z_d)/D_V(z)$, where $r_s(z_d)$ is the sound horizon distance at the drag epoch redshift z_d , when baryons and photons decouple, and $D_V(z)$ is given by:

$$D_V(z) = \left[(1+z)^2 D_A^2(z) \frac{cz}{H(z)} \right]^{1/3}, \quad (5.1)$$

where c is the speed of light. The right panel from Fig. 3 presents the redshift dependence of the variation $\Delta(r_s(z_d)/D_V(z))$ for models sharing the same f_S obtained in the SDP scenario. The figure shows that the BAO measurements break the degeneracy between these models, leading to constraints on sterile neutrino mass and production parameters.

The gravitational lensing of the CMB photons provides direct measurements on scales where the effects of sterile neutrino are expected to manifest. The largest scale affected is the present value of co-moving free-streaming horizon given by [110]:

$$\lambda_{fsh}^0 = \int_{T_0}^{T_{\text{prod}}} \frac{\langle v(T) \rangle}{a(T)} \frac{dt}{dT} dT, \quad (5.2)$$

where $\langle v(T) \rangle$ is the velocity dispersion of sterile neutrinos, T_{prod} is the sterile neutrino production temperature and T_0 is the present temperature. We compute λ_{fsh}^0 for RP and SDP models following the analytical approach from Ref. [110]:

$$\lambda_{fsh}^0 = \frac{a_{nr}}{\sqrt{\Omega_R} H_0} \left(1 + 6 \text{Arcsinh} \sqrt{\frac{a_{eq}}{a_{nr}}} \right), \quad (5.3)$$

where $a_{eq} = \Omega_R/\Omega_m$ is the scale factor at matter-radiation equality, $a_{nr} = T_0/m_{\nu_s}$ is the scale factor at the time of sterile neutrino non-relativistic transition, Ω_R is the radiation energy density and Ω_m is the matter energy density. The analytical approach (5.3) assumes that Universe is completely radiation dominated until a_{eq} and neglects the small contribution to the integral (5.2) of the dark energy. We account for the entropy dilution from T_{prod} until T_0 rescaling λ_{fsh}^0 by a factor $\xi_s^{1/3} = g_s(T_{\text{prod}})/g_s(T_0)$ [55], where g_s is the effective number relativistic entropy degrees of freedom ($g_s(T_{\text{QCD}}) \approx 38.1$ for RP, $g_s(T_{\text{EWFT}}) \approx 109.5$ for SDP and $g_s(T_0) \approx 3.36$) and take into account the increase of Ω_R in RP model according to Eq.(3.1).

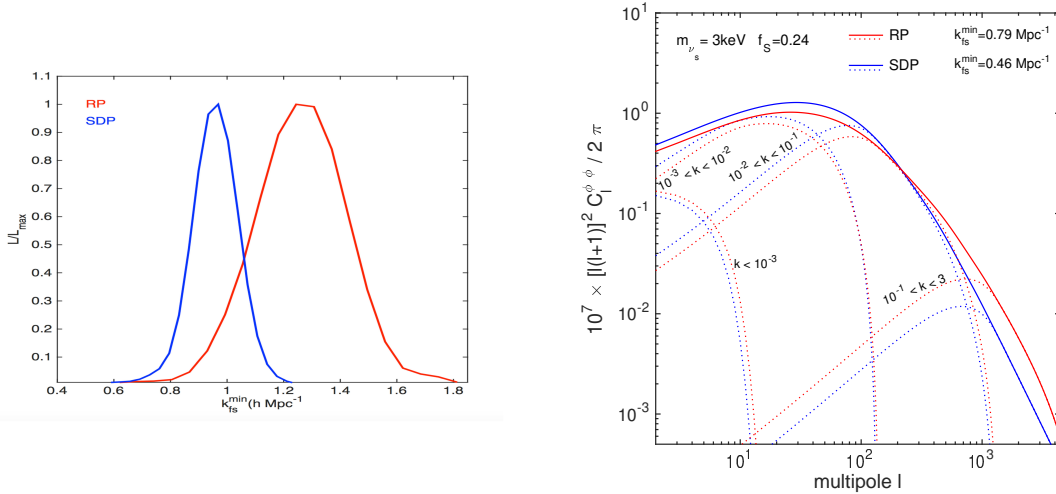


Figure 4: *Left:* The likelihood probability distributions of the estimated free-streaming horizon wave-number, k_{fs}^{min} , from the fit of RP and SDP models with PLANCK+lens+BAO+DES datasets. *Right:* The deflection angle power spectra for models sharing the same values of f_s and m_{ν_s} obtained in RP and SDP scenarios. The contributions of different wave numbers k (in Mpc^{-1}) to the deflection angle power spectra are also presented (dotted lines). RP and SDP mechanism parameters are indicated in Fig. 3. Other parameters are fixed to: $\Omega_b h^2 = 0.0226$, $\Omega_c h^2 = 0.112$, $\Omega_\nu h^2 = 0.00064$, $H_0 = 70 \text{ km s}^{-1} \text{Mpc}^{-1}$ and $\Omega_K = 0$.

Left panel from Fig. 4 presents the likelihood probability distributions of the free-streaming horizon wave-number k_{fs}^{min} , obtained for our models. One should note that wave-numbers $k \sim 1 \text{ hMpc}^{-1}$ correspond to the typical size of dwarf galaxies [66], while the observations of Ly- α absorption in spectra of distant quasars are tracers of linear density fluctuations on scales $0.1 < k < 3 \text{ hMpc}^{-1}$ [111].

On the other hand, the power spectrum of the CMB projected gravitational potential, $C_l^{\phi\phi}$, is sensitive to both geometry and growth of structures at wave-numbers $k > k_{fs}^{min}$. In the Limber approximation, $C_l^{\phi\phi}$ can be written as:

$$C_l^{\phi\phi} = \frac{8\pi}{l^3} \int_0^{\chi^*} d\chi D_A(\chi) \left(\frac{D_A(\chi^*) - D_A(\chi)}{D_A(\chi^*) D_A(\chi)} \right)^2 P_\Psi(z(\chi), k = l/D_A(\chi)), \quad (5.4)$$

where: χ is the co-moving coordinate distance, χ^* is the co-moving coordinate distance to the last scattering surface, k is the wave-number, $D_A(\chi)$ is the co-moving angular diameter distance and $P_\Psi(z, k)$ is the power spectrum of the gravitational potential. $P_\Psi(z, k)$ can be related to the power spectrum of matter density fluctuations, $P_m(z, k)$, through the Poisson equation, leading to [112]:

$$P_\Psi(z, k) = \frac{9\Omega_m^2(\chi) H^4(\chi) P_m(z, k)}{8\pi^2 k}, \quad (5.5)$$

where k is in units of Mpc^{-1} and $P_m(k, z)$ is in units of Mpc^3 . The deflection angle power spectrum of the CMB lensing potential, as reported from the PLANCK CMB lensing analysis [113], is then given by $l^2(l+1)^2 C_l^{\phi\phi}$.

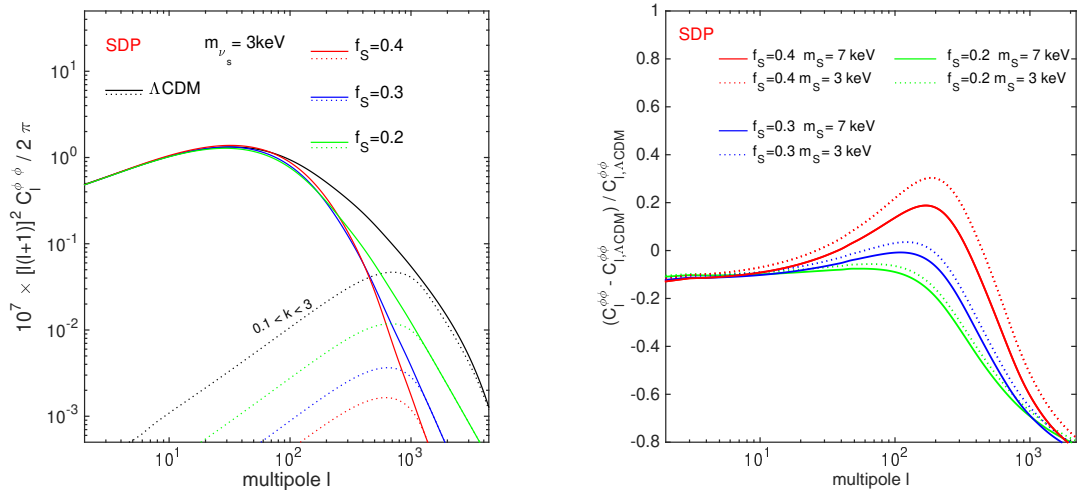


Figure 5: *Left:* The dependence of the deflection angle power spectra on sterile neutrino mass fraction f_S in models sharing the same sterile neutrino mass m_{ν_s} , obtained in SDP scenario. For comparison we plot the deflection angle power spectrum for Λ CDM model. The contributions of the wave numbers in the range $0.1 < k < 3 \text{ Mpc}^{-1}$ are also indicated (dotted lines). *Right:* Fractional differences between $C_l^{\phi\phi}$ obtained in SDP scenario and in Λ CDM model. The SDP mechanism parameters are indicated in Fig. 3. Other parameters are fixed to: $\Omega_b h^2 = 0.0226$, $\Omega_c h^2 = 0.112$, $\Omega_\nu h^2 = 0.00064$, $H_0 = 70 \text{ km s}^{-1} \text{ Mpc}^{-1}$ and $\Omega_K = 0$.

The right panel from Fig. 4 presents the deflection angle power spectra obtained for models sharing the same values of f_S and m_{ν_s} obtained in RP and SDP scenarios. We indicate the contributions of different wave-numbers k (in Mpc^{-1}) to the deflection angle power spectra. The figure shows that for multipole range involved in this analysis, $40 \leq l \leq 400$, the deflection angle power spectrum of the CMB lensing potential is sensitive to both sterile neutrino production mechanisms, with an increased value of the wave-number of power suppression in the RP case. Depending on both angular diameter distance and matter density fluctuations, $C_l^{\phi\phi}$ can break the degeneracy between m_{ν_s} and f_S . This can be seen explicitly in Fig. 5 where we show the dependences of $C_l^{\phi\phi}$ on f_S for models sharing the same m_{ν_s} (left) and the fractional differences between $C_l^{\phi\phi}$ in Λ CDM model and in models sharing the same f_S and different m_{ν_s} (right).

The observations of galaxy shear due to gravitational lensing can achieve similar sensitivity at lower redshifts than the CMB gravitational lensing [114].

We conclude in Fig. 6 that PLANCK+lens+BAO+DES datasets have enough sensitivity to constrain the sterile neutrino mass and mass fraction inside the co-moving free-streaming horizon in both RP and SDP scenarios.

5.2 Constraints on sterile neutrino DM production parameters

RP case: Fig. 7 presents the likelihood probability distributions and the joint confidence regions obtained for the RP mechanism parameters. The dominant effect on sterile neutrino

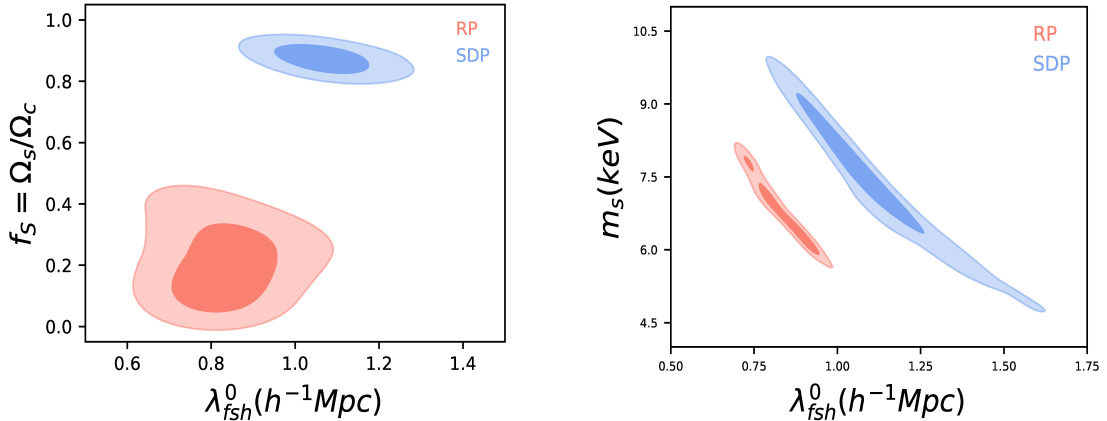


Figure 6: *Left:* The marginalised likelihood posterior distributions (at 68% and 95% C.L.) in λ_{fsh}^0 - f_S plane from the fit of RP and SDP models with PLANCK+LENS+BAO+DES datasets. *Right:* The same distributions in λ_{fsh}^0 - m_{ν_s} plane.

resonant production is given by $\nu/\bar{\nu}$ chemical potential ζ_{ν_α} , that sets the initial lepton number L_{ν_α} , which in turn sets the matter mixing angle $\sin^2 2\theta$ to get the sterile neutrino mass m_{ν_s} . The best fit values of RP parameters lead to $f_S = 0.28 \pm 0.3$ (68% C.L.), indicating that RP is a subdominant mechanism. We find that m_{ν_s} and $\sin^2 2\theta$ are in the parameter space of interest for DM decay interpretation of the 3.5 keV X-ray line [44].

SDP case: Fig. 8 presents the likelihood probability distributions and the joint confidence regions obtained for the SDP mechanism parameters. The dominant effect on SDP production is given by the strength of the Higgs coupling, λ_H , that sets M_S , and by the strength of Yukawa coupling, y_k , that sets the m_{ν_s} . The best fit values of SDP parameters lead to $f_S = 0.86 \pm 0.07$ (68% C.L.), indicating that SDP is a dominant mechanism.

Sterile neutrino mass predicted by RP and SDP mechanisms are consistent within 0.3σ

5.3 Cosmological predictions of sterile neutrino production mechanisms

5.3.1 Acoustic scales

As shown in the previous section, a tight constraint on the ratio θ_d/θ_s implies a tight constraint on the radiation energy density at photon decoupling, parametrised by number of relativistic degrees of freedom, N_{eff} [115]. We find that the values of N_{eff} obtained in RP and SDP scenarios are consistent with the SM value of N_{eff} within 1.8σ and 1.5σ respectively. Left panel from Fig. 9 shows that RP and SDP mechanisms are consistent within less than 1σ in the θ_d/θ_s - N_{eff} plane.

Motivated by the fact that $\Omega_m h^3$ is a well determined parameter orthogonal to the acoustic scale degeneracy in the flat cosmologies [116, 117], we present in the right panel from Fig. 9 the confidence regions in θ_s - $\Omega_m h^3$ plane showing that RP and SDP mechanisms are also consistent within less than 1σ .

5.3.2 Small-scale fluctuations

The amplitude of the CMB acoustic Doppler peaks is exponentially suppressed on scales smaller than the Hubble radius at reionization due to the Thomson scattering of the free

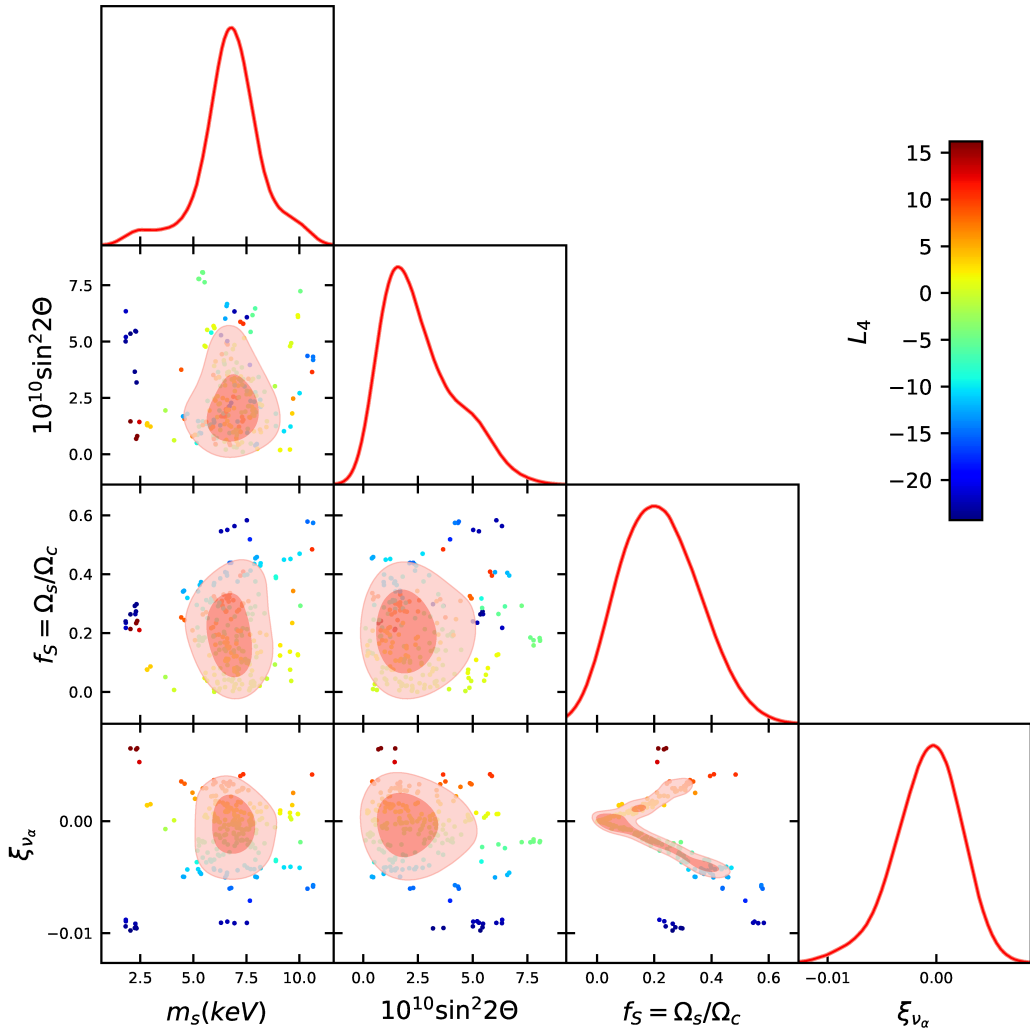


Figure 7: The marginalised likelihood probability distributions and the joint confidence regions (68% and 95% CL) for RP mechanism parameters colour-coded by the values of the initial lepton number $L_4 = 10^4 L_{\nu_\alpha}$. The dominant effect on sterile neutrino RP production is given by the lepton asymmetry L_{ν_α} , that sets the matter mixing angle $\sin^2 2\theta$ to get a sterile neutrino mass, m_{ν_s} . The best fit values of RP model parameters lead to $f_S = 0.28 \pm 0.3$ (68% C.L.), indicating that RP is a subdominant mechanism. The sterile neutrino mass and the mixing angle are in the parameter space of interest for DM decay interpretation of the 3.5 keV X-ray line [44].

electrons produced at this epoch. The amount of this suppression is given by $e^{-2\tau}$, where τ is the optical depth of the CMB photons. PLANCK high precision measurements of the CMB anisotropy at small scales accurately constrain the damped amplitude while the CMB lensing potential power spectrum provides the determination of the amplitude independent on the optical depth [2, 3]. As the CMB power spectrum constrains the matter density fluctuations along the line of sight, the present-day *rms* matter density power, σ_8 , is also determined. The CMB small-scale power fluctuations directly fixes the combination $\sigma_8 e^{-\tau}$ that is tightly

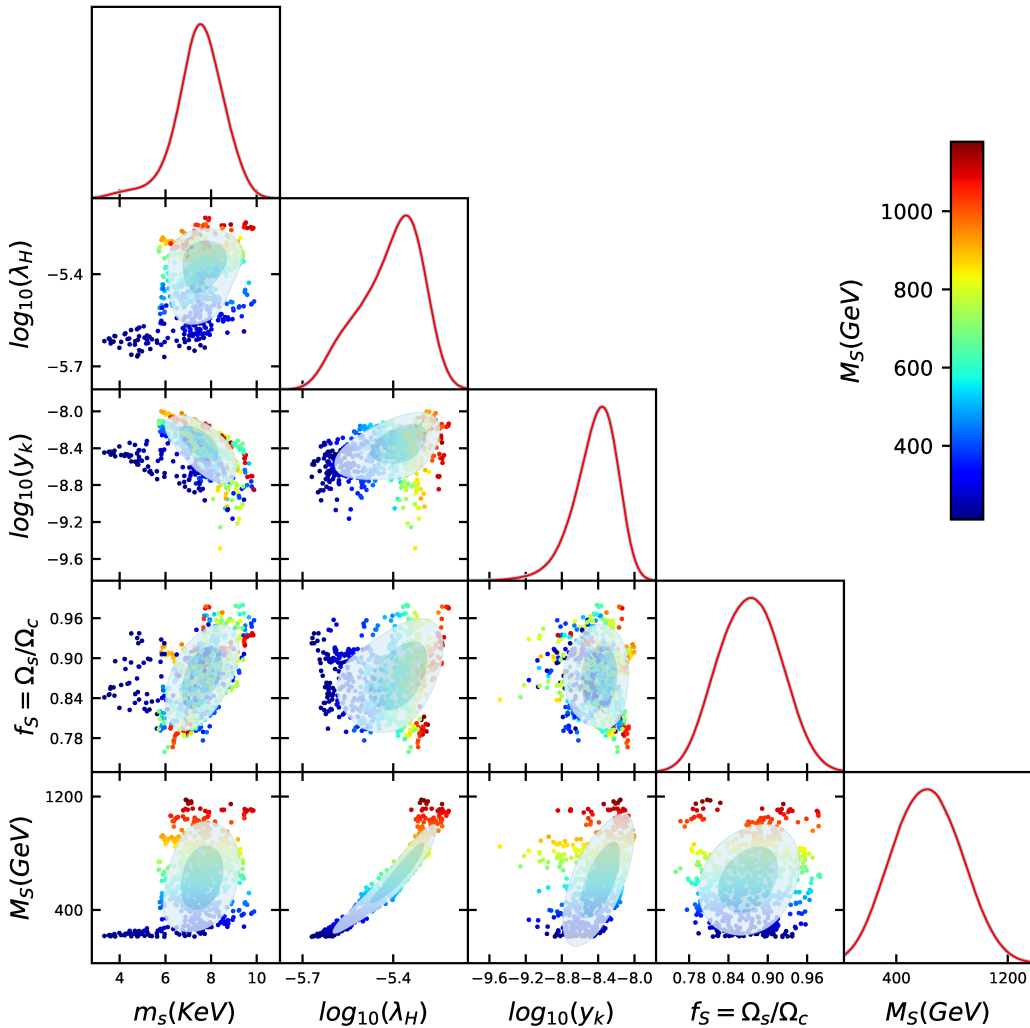


Figure 8: The marginalised likelihood probability distributions and the joint confidence regions (68% and 95% CL) for SDP mechanism parameters colour-coded by the scalar mass values M_S . The dominant effect on SDP mechanism is given by the strength of the Higgs coupling, λ_H , that sets M_S , and the strength of Yukawa coupling, y_k , that sets m_{ν_s} . The best fit values of the SDP parameters lead to $f_S = 0.86 \pm 0.07$ (68% C.L.), indicating that SDP is a dominant mechanism. Sterile neutrino mass predicted by RP and SDP mechanisms are consistent within 0.3σ .

constrained by the data [4].

Also, the weak gravitation lensing of galaxies (cosmic shear) is sensitive to the matter fluctuations at small-scales, providing constraints on the combination $S_8 \equiv \sigma_8(\Omega_m/0.3)^{0.5}$ [107]. Fig. 10 illustrates the degree of consistency between the sterile neutrino RP and SDP mechanisms and the Λ CDM-ext model at small-scales. The left panel shows the impact of $\sigma_8 e^{-\tau}$ and Ω_m . The RP and SDP models prefer higher values of $\sigma_8 e^{-\tau}$ that make them distinguishable from Λ CDM-ext at 1.2σ level. In the right panel of the same figure we show the impact of $S_8 \equiv \sigma_8(\Omega_m/0.3)^{0.5}$ and the Hubble parameter H_0 . The value of $S_8 = 0.792 \pm 0.024$ (68%

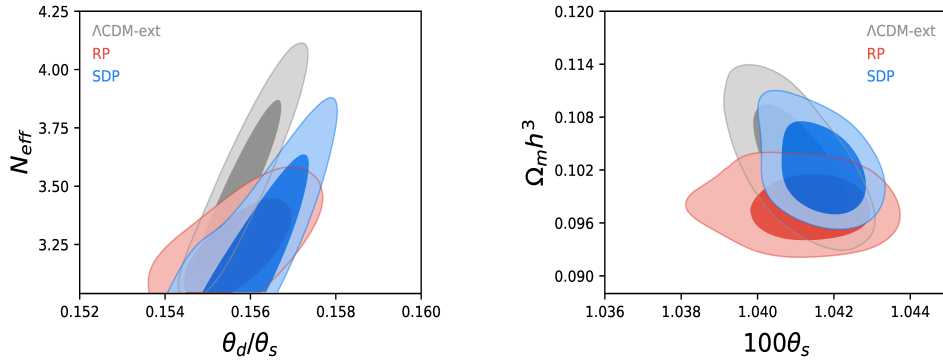


Figure 9: The role of the acoustic scale measurements to discriminate the sterile neutrino DM production mechanisms. The contours show the 68% and 95% C.L. *Left:* The confidence regions in $\theta_d/\theta_s - N_{eff}$ plane showing that RP and SDP mechanisms are consistent within less than 1σ . *Right:* The confidence regions in $\theta_s - \Omega_m h^3$ plane showing that RP and SDP mechanisms are also consistent within less than 1σ .

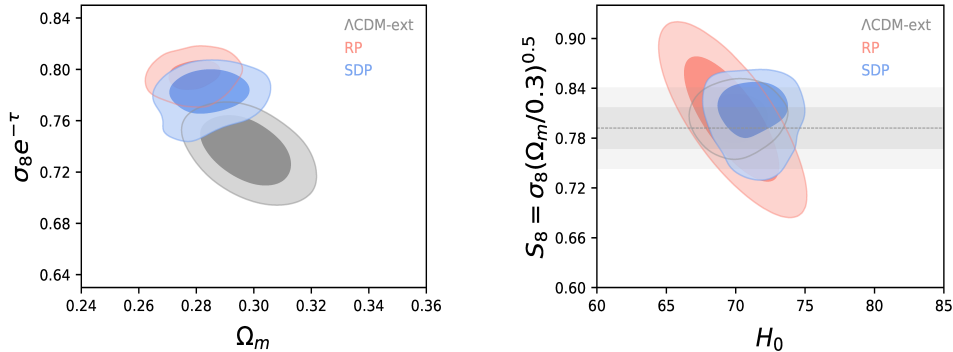


Figure 10: The degree of consistency between sterile neutrino RP and SDP mechanisms and the Λ CDM-ext model at small-scales. The contours show the 68% and 95% C.L. *Left:* The impact of $\sigma_8 e^{-\tau}$ and Ω_m . The RP and SDP models prefer higher values of $\sigma_8 e^{-\tau}$ that make them distinguishable from Λ CDM-ext model at more than 1σ . *Right:* The impact of $S_8 \equiv \sigma_8 (\Omega_m/0.3)^{0.5}$ and Hubble parameter H_0 . The horizontal dashed line and the grey band mark the central value and $\pm 2\sigma$ error of S_8 value determined by DES survey from the combined clustering and lensing measurements [107].

C.L.) obtained by DES survey from the combined clustering and lensing measurements [107] is also indicated. We find that S_8 values obtained in RP and SDP scenarios are consistent with that determined by DES within 0.6σ and 1.5σ respectively.

5.3.3 Low-redshift geometric probes

We consider the low-redshift geometric probes, BAO and Hubble parameter H_0 , to constrain the sterile neutrino DM production mechanisms. We evaluate the characteristic BAO parameter (5.1) at $z_{eff} = 0.57$ reported by the BOSS DR11 survey [100]. Left panel from Fig. 11 presents constraints on our models in $H_0 - r_s/D_V(z_{eff})$ plane. The horizontal dashed line

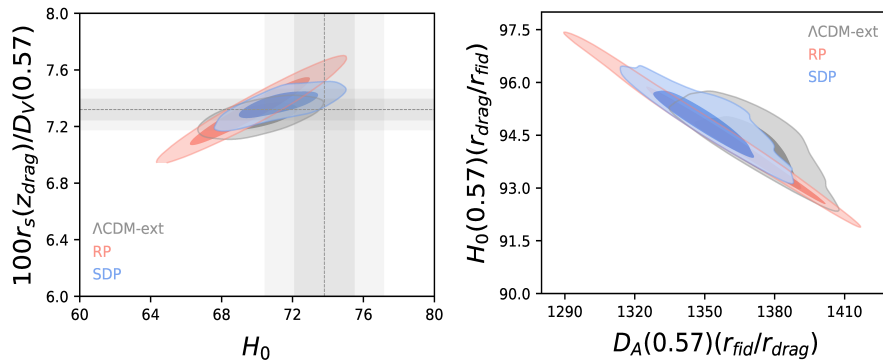


Figure 11: The role of the low-redshift geometric probes to discriminate between the sterile neutrino DM production mechanisms. The contours show the 68% and 95% C.L.

Left: The impact of Hubble parameter H_0 and of the BAO characteristic parameter $r_s/D_V(z_{eff})$. The horizontal dashed line and the grey bands mark the central value and $\pm 1\sigma$ and $\pm 2\sigma$ errors of the BOSS measurement at $z_{eff} = 0.57$ [100], while the vertical dashed line and the grey bands do the same for H_0 determination from SHOES experiment [119]. *Right:* The role of BAO measurements on line-of-sight and transverse directions, leading to joint constraints of $D_A(z_{eff})/r_{drag}$ and $H_0(z_{eff})r_{drag}$. We take the fiducial sound horizon distance at the drag epoch $r_{fid}=147.78$ Mpc [102].

and the grey bands mark the central value and $\pm 1\sigma$ and $\pm 2\sigma$ errors of the BOSS measurement while the vertical dashed line and the grey bands do the same for H_0 determination from SHOES experiment [119].

On the other hand, the BAO features in the galaxy correlation function can be measured in both line-of-sight and transverse directions, leading to joint constraints on the angular diameter distance and the Hubble parameter at z_{eff} [100]. Taking the fiducial sound horizon distance at the drag epoch $r_{fid}=147.78$ Mpc [102], we compute the constraints on our models in $D_A(z_{eff})r_{fid}/r_{drag} - H_0(z_{eff})r_{drag}/r_{fid}$ plane. The the join confidence regions are presented in the right panel from Fig. 11.

We conclude that present low-redshift geometric probes like BAO and H_0 start to discriminate between the sterile neutrino RP and SDP mechanisms. However, the SDP scenario remains consistent with Λ CDM-ext model within less than 1σ .

6 Conclusions

In this paper we place constraints on sterile neutrino RP and SDP mechanisms assuming that sterile neutrino represents a fraction f_s from the total CDM energy density.

So far, the keV sterile neutrino properties have been addressed under the assumption that sterile neutrinos are all of the DM, by evaluating their impact on the co-moving free streaming horizon that relates on the average velocity distribution. For such models, characterised by highly non-thermal momentum distributions, the average momentum is subject of uncertainties, leading to the fail of free-streaming horizon in constraining their parameters.

For our cosmological analysis, we complement the CMB anisotropies measurements with CMB lensing gravitational potential measurements, that are sensitive to the DM distribution out to high redshifts and with the cosmic shear data, that constraints the gravitational

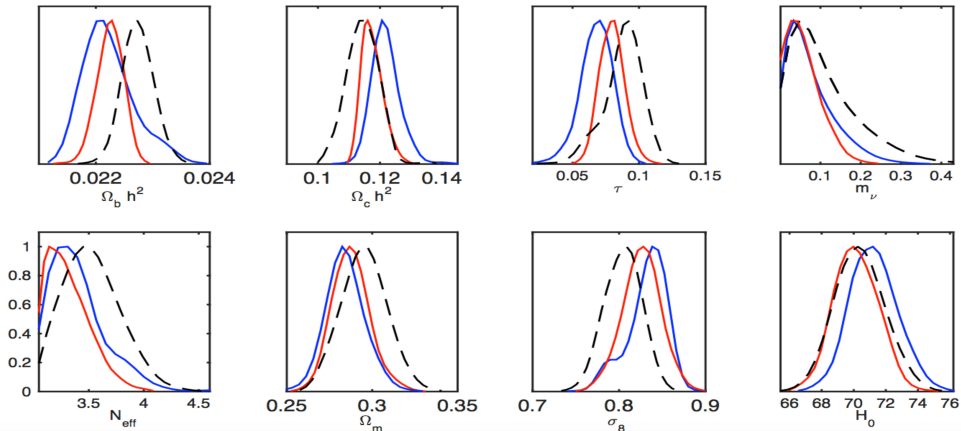


Figure 12: The marginalised likelihood probability distributions obtained from the fit with PLANCK+lens+BAO+DES datasets of the Λ CDM-ext model (black dashed lines), RP model (red lines) and SDP model (blue lines).

potential at lower redshifts than CMB. We also use the most recent low-redshift BAO measurements that are insensitive to the non-linear effects, providing robust geometrical tests.

We show that for models sharing the same f_S , the accurate determination of the acoustic scale from CMB anisotropy measurements breaks the degeneracy of Hubble parameter at the photon decoupling, constraining m_{ν_s} in RP scenario, while the BAO measurements constrain m_{ν_s} at lower redshifts. We evaluate the co-moving free-streaming horizon for RP and SDP models showing that, the deflection angle power spectrum of the CMB lensing potential, $C_l^{\phi phi}$ is sensitive to both sterile neutrino production mechanisms for the multipole range involved in this analysis ($40 \leq l \leq 400$) with the increased wave-number of power suppression in RP case. Depending on both angular diameter distance and matter density fluctuations, we show that $C_l^{\phi phi}$ can break the degeneracy between f_S and m_{ν_s} in our models. We also show that our datasets have enough sensitivity to constrain the sterile neutrino mass and mass fraction inside the co-moving free-streaming horizon in both RP and SDP scenarios. The best fit parameters obtained from our cosmological analysis are presented in Tab. 3 and Fig. 12. For RP case we find that the best fit values of m_{ν_s} and $\sin^2 \theta$ are in the parameter space of interest for sterile neutrino DM decay interpretation of the 3.5 keV X-ray line with a DM mass fraction $f_S = 0.28 \pm 0.3$ (at 68% CL) that excludes the assumption of sterile neutrinos as being all of the DM. For SDP case we find $f_S = 0.86 \pm 0.07$ (at 68% CL), in agreement with the upper limit constraint on f_S from the X-ray non-detection and Ly- α forest measurements that rejects $f_S = 1$ at 3σ level [1].

The sterile neutrino mass predicted by both RP and SDP models are consistent within 0.3σ . We analysed the possibility to distinguish between RP and SDP scenarios through their impact on the acoustic scales, the small scale fluctuations and the low-redshift geometric observ-

Table 3: The table shows the mean values and the absolute errors of the main parameters obtained from the fit of Λ CDM-ext, RP and SDP models with the data-sets. The errors are quoted at 68% C.L. The upper limits are quoted at 95% C.L. The first group of parameters are the base cosmological parameters sampled in the Monte-Carlo Markov Chains analysis with uniform priors. The others are derived parameters.

Parameter	Λ CDM-ext	RP	SDP
$\Omega_b h^2$	0.0223 ± 0.0002	0.0222 ± 0.0003	0.0219 ± 0.0003
$\Omega_c h^2$	0.122 ± 0.004	0.118 ± 0.003	0.121 ± 0.004
$100\theta_{MC}$	1.0412 ± 0.0008	1.0404 ± 0.0011	1.0413 ± 0.0009
τ	0.087 ± 0.015	0.079 ± 0.009	0.069 ± 0.012
$\sum m_\nu$	< 0.321	< 0.249	< 0.198
N_{eff}	3.520 ± 0.259	3.313 ± 0.109	3.380 ± 0.243
f_S		0.281 ± 0.03	0.860 ± 0.071
$\sin^2 2\theta$		2.460 ± 1.750	
$10^3 \zeta_{\nu\alpha}$		-0.822 ± 2.691	
M_S (GeV)			533.60 ± 47.21
$10^{-6} \lambda_H$			3.780 ± 0.642
$10^{-9} y_k$			3.451 ± 1.820
Ω_m	0.295 ± 0.013	0.287 ± 0.011	0.284 ± 0.011
σ_8	0.808 ± 0.021	0.801 ± 0.022	0.832 ± 0.019
H_0	70.512 ± 1.556	70.142 ± 1.355	71.210 ± 1.433
m_{ν_s} (keV)		6.831 ± 1.630	7.882 ± 0.731
$L_4 = 10^4 L_{\nu\alpha}$		-2.081 ± 6.710	
$100\theta_s$	1.0411 ± 0.0002	1.0391 ± 0.0011	1.0421 ± 0.0011
$100\theta_d$	0.1622 ± 0.0002	0.1619 ± 0.0061	0.1632 ± 0.0011

ables, obtaining cosmological constraints that clearly show that the present-day cosmological data start to discriminate between different sterile neutrino DM production mechanisms. However, we expect the future BAO and weak lensing surveys, such as EUCLID, to provide much robust constraints.

Acknowledgments

This work was partially supported by UEFISCDI Contract 18PCCDI/2018. We also acknowledge the use of the GRID computing system facility at the Institute of Space Science Bucharest and would like to thank the staff working there.

References

- [1] A., Palazzo, D. Cumberbatch, A. Slosar, J. Silk, J., Sterile neutrinos as subdominant warm dark matter, *Phys. Rev. D* **76** (2007) 103511 [arXiv:0707.1495].

- [2] Planck Collaboration; P. A. R. Ade et al., *Planck 2013 results. XVI. Cosmological Parameters, A & A* **571** (2014) 66 [arXiv:1303.5076].
- [3] Planck Collaboration; P. A. R. Ade et al., *Planck 2015 results. XIII. Cosmological Parameters, Astronomy & Astrophysics* **594** (2016) 63 [arXiv:1502.01589].
- [4] Planck Collaboration; N. Aghanim et al., *Planck 2018 results. VI. Cosmological parameters*, (2018) [arXiv:1807.06209].
- [5] A. G. Riess et al., *A 3% Solution: Determination of the Hubble Constant with the Hubble Space Telescope and Wide Field Camera 3*, *The Astrophysical Journal* **730** (2011) 119 [arXiv:astro-ph/1103.2976].
- [6] W. L. Freedman et al., *Carnegie Hubble Program: A Mid-Infrared Calibration of the Hubble Constant* *The Astrophysical Journal* **758** 24 (2012) [arXiv:astro-ph/1208.3281].
- [7] S. H. Suyu, M. W. Auger, S. Hilbert, et al., *Two accurate time-delay distances from strong lensing: Implications for cosmology*, *The Astrophysical Journal* **766** 70 (2013) [arXiv:astro-ph/1208.6010].
- [8] A. Vikhlinin, A. V. Kravtsov, R. A. Burenin et al., *Chandra Cluster Cosmology Project III: Cosmological Parameter Constraints*, *The Astrophysical Journal* **692** (2009) 1060 [arXiv:astro-ph/0812.2720].
- [9] H. Bohringer, G. Chon and C. A. Collins, *The extended ROSAT-ESO Flux Limited X-ray Galaxy Cluster Survey (REFLEX II) IV. X-ray Luminosity Function and First Constraints on Cosmological Parameters*, *Astronomy & Astrophysics* **570** (2014) 31 [arXiv:astro-ph/1403.2927].
- [10] V. Marra, L. Amendola, I. Sawicki, W. Valkenburg, *Cosmic Variance and the Measurement of the Local Hubble Parameter*, *Phys. Rev. Lett.* **110** (2013) 241305 [arXiv:astro-ph/1303.3121].
- [11] Z. Berezhiani, A. D. Dolgov, I. I. Tkachev, *Reconciling Planck results with low redshift astronomical measurements*, *Phys. Rev.* **D92** 061303 [arXiv:1505.03644].
- [12] S. Weinberg, *The cosmological constant problem*, *Rev. Mod. Phys.* **61** 1 (1989).
- [13] L. P. Chimento, A. S. Jakubi, D. Pavon, and W. Zimdahl, *Dark energy, dissipation, and the coincidence problem*, *Phys. Rev.* **D67** (2003) 083513 [arXiv:astro-ph/0303145].
- [14] B. Ratra and P. J. E. Peebles, *Cosmological consequences of a rolling homogeneous scalar field*, *Phys. Rev.* **D37** (1998) 3406.
- [15] S. Matarrese, C. Baccigalupi and F. Perrotta, *Approaching Λ without fine-tuning*, *Phys. Rev.* **D70** 061301 (2004) [arXiv:astro-ph/0403480].
- [16] L. Amendola and S. Tsujikawa, *Dark Energy: Theory and Observations*, ed. Cambridge University Press (2010).
- [17] P. J. E. Peebles and B. Ratra, *Cosmology with a time-variable cosmological 'constant'*, *Astrophysical Journal. Lett.* **325**, L17-L20.
- [18] I. L. Shapiro and J. Sola, *On the possible running of the cosmological 'constant'*, *Phys. Lett.* **B682** 105 (2009) [arXiv:astro-ph/0910.4925].
- [19] J. Sola, *Dark energy: a quantum fossil from the inflationary universe?*, *Journal of Physics* **A41** 164066 (2008) [arXiv:astro-ph/0710.4151].
- [20] A. Klypin, A. V. Kravtsov, O. Valenzuela, F. Prada, *Where Are the Missing Galactic Satellites?*, *The Astrophysical Journal* **522** (1999) 82 [arXiv:astro-ph/9901240].
- [21] M. A. Zwaan, M. J. Meyer, L. Staveley-Smith, *The velocity function of gas-rich galaxies*, *Monthly Notices of the Royal Astronomical Society* **403** (2010) 1969 [arXiv:0912.1754].
- [22] E. Papastergis, A. M. Martin, R. Giovanelli, M. P. Haynes, *The Velocity Width Function of*

- Galaxies from the 40% ALFALFA Survey: Shedding Light on the Cold Dark Matter Overabundance Problem*, *The Astrophysical Journal* **739** (2011) 38 [arXiv:1106.0710].
- [23] P. Salucci, A. Burkert, *Dark Matter Scaling Relations*, *The Astrophysical Journal* **737** (2000) 9 [arXiv:astro-ph/0004397].
- [24] G. Gentile, P. Salucci, U. Klein, D. Vergani, P. Kalberla, *The cored distribution of dark matter in spiral galaxies*, *Monthly Notices of the Royal Astronomical Society* **351** (2004) 903 [arXiv:astro-ph/0403154].
- [25] R. Kuzio de Naray, T. Kaufmann, *Recovering cores and cusps in dark matter haloes using mock velocity field observations*, *Monthly Notices of the Royal Astronomical Society* **414** (2011) 3617 [arXiv:1012.3471].
- [26] M. Boylan-Kolchin, J. S. Bullock, M. Kaplinghat, *Too big to fail? The puzzling darkness of massive Milky Way subhaloes*, *Monthly Notices of the Royal Astronomical Society* **415** (2011) L40 [arXiv:1103.0007].
- [27] M. Boylan-Kolchin, J. S. Bullock, M. Kaplinghat, *The Milky Way's bright satellites as an apparent failure of CDM*, *Monthly Notices of the Royal Astronomical Society* **422** (2012) 1203 [arXiv:1111.2048].
- [28] G. Jungman, M. Kamionkowski, K. Griest, *Supersymmetric dark matter*, *Physical Reports* **267** (1996) 195 [arXiv:hep-ph/9506380].
- [29] G. Bertone, D. Hooper, J. Silk, *Particle dark matter: evidence, candidates and constraints*, *Physical Reports* **405** (2005) 279 [arXiv:hep-ph/0404175].
- [30] J. L. Feng, *Dark Matter Candidates from Particle Physics and Methods of Detection*, *Ann. Rev. Astron. Astrophys.* **48** (2010) 495 [arXiv:1003.0904].
- [31] P. Gondolo and G. Gelmini, *Cosmic abundances of stable particles: Improved analysis*, *Nuclear Physics* **B360** (1991) 145.
- [32] R. Adhikari, M. Agostini, N. A. Ky, T. Araki et al, *JCAP* **1701** (2017) 025 [arXiv:1602.04816].
- [33] K.N. Abazajian, G.M. Fuller and M. Patel, *Sterile neutrino hot, warm and cold dark matter*, *Phys. Rev. D* **64** (2001) 023501 [astro-ph/0101524].
- [34] K.N. Abazajian and G.M. Fuller, *Bulk QCD thermodynamics and sterile neutrino dark matter*, *Phys. Rev. D* **66** (2002) 023526 [astro-ph/0204293].
- [35] A. Boyarsky, O. Ruchayskiy and M. Shaposhnikov, *The Role of sterile neutrinos in cosmology and astrophysics*, *Ann. Rev. Nucl. Part. Sci.* **59** (2009) 191 [arXiv:0901.0011].
- [36] A. Kusenko, *Sterile neutrinos: The Dark side of the light fermions*, *Physical Reports* **481** (2009) 1 [arXiv:0906.2968].
- [37] T. Asaka, S. Blanchet and M. Shaposhnikov, *The MSW dark matter and neutrino masses*, *Phys. Lett. B* **631** (2005) 151 [hep-ph/0503065].
- [38] T. Asaka and M. Shaposhnikov, *The MSM, dark matter and baryon asymmetry of the universe*, *Phys. Lett. B* **620** (2005) 17 [hep-ph/0505013].
- [39] E. Bulbul, M. Markevitch, A.R. Foster, R.K. Smith, M. Loewenstein and S.W. Randall, *Detection of An Unidentified Emission Line in the Stacked X-ray spectrum of Galaxy Clusters*, *The Astrophysical Journal* **789** (2014) 13 [arXiv:1402.2301].
- [40] A. Boyarsky, O. Ruchayskiy, D. Iakubovskiy and J. Franse, *Unidentified Line in X-Ray Spectra of the Andromeda Galaxy and Perseus Galaxy Cluster*, *Phys. Rev. Lett.* **113** (2014) 251301 [arXiv:1402.4119].
- [41] E. Bulbul, M. Markevitch, A.R. Foster, R.K. Smith, M. Loewenstein and S.W. Randall, *Detection of an Unidentified Emission Line in the Stacked X-Ray Spectrum of Galaxy*

- Clusters, The Astrophysical Journal* **789**, (2014) [arXiv: 1402.2301].
- [42] A. Boyarsky, J. Franse, D. Iakubovskiy and O. Ruchayskiy, *Comment on the paper “Dark matter searches going bananas: the contribution of Potassium (and Chlorine) to the 3:5 keV line” by T. Jeltema and S. Profumo* [arXiv:1408.4388].
- [43] E. Carlson, T. Jeltema and S. Profumo, *Where do the 3:5 keV photons come from? A morphological study of the Galactic Center and of Perseus*, *JCAP* **02** (2015) 009 [arXiv:1411.1758].
- [44] K.N. Abazajian, G.M. Fuller and M. Patel, *Sterile neutrino hot, warm and cold dark matter*, *Phys. Rev. D* **64** (2001) 023501 [astro-ph/0101524].
- [45] L. J. Hall, K. Jedamzik, J. March-Russell, S. M. West, *Freeze-in production of FIMP dark matter*, *JHEP* **1003** (2010) 080 [arXiv:0911.1120].
- [46] S. Dodelson and L.M. Widrow, *Sterile-neutrinos as dark matter*, *Phys. Rev. Lett.* **72** (1994) 17 [hep-ph/9303287].
- [47] L. Canetti, M. Drewes, T. Frossard, M. Shaposhnikov, *Dark matter, baryogenesis and neutrino oscillations from right-handed neutrinos*, *Phys. Rev. D* **87** (2013) 093006 [arXiv:1208.4607].
- [48] A. Merle and V. Niro, *Influence of a keV sterile neutrino on neutrinoless double beta decay: How things changed in recent years* *Phys. Rev. D* **88** (2013) 113004 [arXiv: 1302.2032].
- [49] X.-D. Shi and G.M. Fuller, *A New dark matter candidate: Nonthermal sterile neutrinos*, *Phys. Rev. Lett.* **82** (1999) 2832 [astro-ph/9810076].
- [50] K.N. Abazajian, G.M. Fuller and M. Patel, *Sterile neutrino hot, warm and cold dark matter*, *Phys. Rev. D* **64** (2001) 023501 [astro-ph/0101524].
- [51] K.N. Abazajian and G.M. Fuller, *Bulk QCD thermodynamics and sterile neutrino dark matter*, *Phys. Rev. D* **66** (2002) 023526 [astro-ph/0204293].
- [52] M. Laine and M. Shaposhnikov, *Sterile neutrino dark matter as a consequence of MSM-induced lepton asymmetry*, *JCAP* **06** (2008) 031 [arXiv:0804.4543].
- [53] S. Horiuchi, B. Bozek, K. N. Abazajian, et al., *Properties of Resonantly Produced Sterile Neutrino Dark Matter Subhalos*, *Monthly Notices of the Royal Astronomical Society* **456** (2016) 4346 [arXiv:1512.04548].
- [54] M. R. Lovell, S. Bose, A. Boyarsky, et al., *Satellite galaxies in semi-analytic models of galaxy formation with sterile neutrino dark matter*, *Monthly Notices of the Royal Astronomical Society* **461** (2016) 60 [arXiv:1511.04078].
- [55] A. Merle and A. Schneider, *Production of Sterile Neutrino dark matter and the 3.5 keV line*, *Phys. Lett. B* **749** (2015) [arXiv:1409.6311].
- [56] M. Viel, G. D. Becker, J. S. Bolton, and M. G. Haehnelt, *Warm dark matter as a solution to the small scale crisis: New constraints from high redshift Lyman- α forest data*, *Phys. Rev. D* **88** (2013) 043502 [arXiv:1306.2314].
- [57] W. B. Lin, D. H. Huang, X. Zhang, and R. H. Brandenberger, *Nonthermal Production of Weakly Interacting Massive Particles and the Subgalactic Structure of the Universe*, *Phys. Rev. Lett.* **86** (2001) 954 [astro-ph/0009003].
- [58] J. Hisano, K. Kohri, and M. M. Nojiri, *Neutralino warm dark matter*, *Phys. Lett. B* **505**, (2001) 169 [hep-ph/0011216].
- [59] M. Kaplinghat, *Dark matter from early decays*, *Phys. Rev. D* **72** (2005) 063510 [astro-ph/0507300].
- [60] P. Di Bari, S. F. King and A. Merle, *Dark Radiation or Warm Dark Matter from long lived particle decays in the light of Planck*, *Phys. Rev. Lett. B* **724** (2013) 77 [arXiv:1303.6267].

- [61] R. Adhikari, N. A. Ky, T. Akari et al., *A White Paper on keV sterile neutrino Dark Matter* *JCAP* **01** (2017) 025 [arXiv:1602.04816].
- [62] K. Petraki and A. Kusenko, *Dark-matter sterile neutrinos in models with a gauge singlet in the Higgs sector*, *Phys. Rev. D* **77** (2008) 065014 [arXiv:0711.4646].
- [63] A. Kusenko, *Sterile neutrinos, dark matter, and the pulsar velocities in models with a Higgs singlet*, *Phys. Rev. Lett.* **97** (2006) 241301 [hep-ph/0609081].
- [64] A. Kusenko, *Sterile neutrinos: The Dark side of the light fermions*, *Phys. Rept.* **481** (2009) 1 [arXiv:0906.2968].
- [65] A. Merle, V. Niro and D. Schmidt, *New Production Mechanism for keV Sterile Neutrino Dark Matter by Decays of Frozen-In Scalars*, *JCAP* **1403** (2014) 028 [arXiv:1306.3996].
- [66] A. Merle and M. Totzauer, *keV Sterile Neutrino Dark Matter from Singlet Scalar Decays: Basic Concepts and Subtle Features*, *JCAP* **1506** (2015) 011 [1502.01011].
- [67] J. K. Onig, A. Merle, M. Totzauer, *keV sterile neutrino dark matter from singlet scalar decays: the most general case*, *JCAP* **11** (2016) 038 [arXiv:1609.01289].
- [68] A. Merle, A. Schneider and M. Totzauer, *Dodelson-Widrow Production of Sterile Neutrino Dark Matter with Non-Trivial Initial Abundance*, *JCAP* **1604** (2016) 003 [1512.05369].
- [69] M. Shaposhnikov and I. Tkachev, *The ν MSM inflation and dark matter*, *Phys. Lett. B* **639** (2006) 414 [hep-ph/0604236].
- [70] F.L. Bezrukov and D.S. Gorbunov, *Relic Gravity Waves and 7 keV Dark Matter from a GeV scale inflation*, *Phys. Lett. B* **736** (2014) 494 [arXiv:1403.4638].
- [71] L. Lello and D. Boyanovsky, *Phys. Rev. D* **91**(6), 063502 (2015), 1411.2690.
- [72] L. Amendola, V. Pettorino, C. Quercellini, and A. Vollmer, *Phys. Rev. D* **85**, 103008 (2012) [arXiv:1111.1404].
- [73] G. Caldera-Cabral, R. Maartens, and B. M. Schaefer, *The Growth of Structure in Interacting Dark Energy Models*, *JCAP* **0907** (2009) 027 [arXiv:0905.0492].
- [74] L. Amendola, G. Camargo Campos, and R. Rosenfeld, *Consequences of dark matter-dark energy interaction on cosmological parameters derived from SNIa data*, *Phys. Rev. D* **75** (2007) 083506 [astro-ph/0610806].
- [75] G. Izquierdo and D. Pavon, *Limits on the parameters of the equation of state for interacting dark energy*, *Phys. Lett. B* **688** (2010) 115 [arXiv:1004.2360].
- [76] R. Murgia, A. Merle, M. Viel, M. Totzauer, A. Schneider, *Non-cold dark matter at small scales: a general approach*, *JCAP* **11** (2017) 046 [arXiv:1704.07838].
- [77] K.N. Abazajian, *Resonantly Produced 7 keV Sterile Neutrino Dark Matter Models and the Properties of Milky Way Satellites*, *Phys. Rev. Lett.* **112** (2014) 161303 [arXiv:1403.0954].
- [78] O. Wantz and E. P. S. Shellard, *Axion Cosmology Revisited*, *Phys. Rev. D* **82** (2010) 123508, [arXiv:0910.1066].
- [79] D. Boyanovsky, C. Ho, *Sterile neutrino production via active-sterile oscillations: the quantum Zeno effect*, *JHEP* **0707** (2007) 030 [arXiv:hep-ph/0612092].
- [80] L. A. Popa, D. Tonoiu, *Subdominant Dark Matter sterile neutrino resonant production in the light of PLANCK*, *JCAP* **09** (2015) 066 [arXiv:1501.06355].
- [81] K.N. Abazajian, *Resonantly Produced 7 keV Sterile Neutrino Dark Matter Models and the Properties of Milky Way Satellites*, *Phys. Rev. Lett.* **112** (2014) 161303 [arXiv:1403.0954].
- [82] T. Venumadhav, F.-Y. Cyr-Racine, K. N. Abazajian, and C. M. Hirata, *Sterile neutrino dark matter: Weak interactions in the strong coupling epoch*, *Phys. Rev. D* **94** (2016) 043515

- [arXiv:1507.06655]⁴
- [83] J. Ghiglieri and M. Laine, *Improved determination of sterile neutrino dark matter spectrum*, *JHEP* **11** (2015) 171 [arXiv:1506.06752]
- [84] A. Schneider, *Astrophysical constraints on resonantly produced sterile neutrino dark matter*, *JCAP* **04** (2016) 059 [arXiv:1601.07553]
- [85] G. Mangano, G. Miele, S. Pastor, et al., *Relic neutrino decoupling including flavour oscillations*, *Nucl. Phys.* **B 729** (2005) 221 [arXiv:hep-ph/0506164].
- [86] A. Lewis & S. Bridle, *Cosmological parameters from CMB and other data: A Monte Carlo approach*, 2002, *Phys. Rev.* **D 66** (2002) 103511 [arXiv:astro-ph/0205436]
- [87] R. E. Smith, J. A. Peacock, A. Jenkins, et al., *Stable clustering, the halo model and nonlinear cosmological power spectra* *Monthly Notices of the Royal Astronomical Society* **341** (2003) 1311, [arXiv:astro-ph/0207664].
- [88] R. Takahashi, M. Sato, T. Nishimichi, A. Taruya, M. Oguri, *Revising the Halofit Model for the Nonlinear Matter Power Spectrum* *The Astrophysical Journal* **761** 152 (2012) [arXiv:1208.2701].
- [89] S. Seager, D. D. Sasselov, & D. Scott, *A New Calculation of the Recombination Epoch*, 1999, *The Astrophysical Journal* **523** (1999) L1 [arXiv:astro-ph/9909275].
- [90] W. Y. Wong, A. Moss, & D. Scott, *How well do we understand cosmological recombination?*, *Monthly Notices of the Royal Astronomical Society* **386** (2008) 1023 [arXiv:0711.1357]
- [91] K.N. Abazajian, N.F. Bell, G.M. Fuller and Y.Y.Y. Wong, *Cosmological lepton asymmetry, primordial nucleosynthesis and sterile neutrinos*, *Phys. Rev.* **D 72** (2005) 063004 [astro-ph/0410175].
- [92] C.J. Smith, G.M. Fuller, C.T. Kishimoto and K.N. Abazajian, *Light Element Signatures of Sterile Neutrinos and Cosmological Lepton Numbers*, *Phys. Rev.* **D 74** (2006) 085008 [astro-ph/0608377].
- [93] O. Pisanti, A. Cirillo, S. Esposito, et al., *PARthENoPE: Public Algorithm Evaluating the Nucleosynthesis of Primordial Elements*, *Comput. Phys. Commun.* **178** (2008) 956 [arXiv:0705.0290].
- [94] A. Lewis & S. Bridle, *Cosmological parameters from CMB and other data: A Monte Carlo approach*, 2002, *PRD* **66** (2002) 103511 [arXiv:astro-ph/0205436]
- [95] S. Tremaine and J. E. Gunn, *Dynamical role of light neutral leptons in cosmology*, *Phys. Rev. Lett.* **42** (1979) 407.
- [96] A. Palazzo, D. Cumberbatch, A. Slosar, and J. Silk, *Sterile neutrinos as subdominant warm dark matter* *Phys. Rev.* **D76** (2007) [arXiv:0707.1495]
- [97] Planck Collaboration I; R. Adam et al., *Planck 2015 results. I. Overview of products and results*, *Astronomy & Astrophysics*, **594** (2016) [arXiv:1502.01582].
- [98] Planck Collaboration, P. A. R. Ade et al., *Planck 2013 results. XV. CMB power spectra and likelihood*, *A & A* **571** (2016) A11 [arXiv: 1303.5075].
- [99] Planck Collaboration, P. A. R. Ade et al., *Planck 2015 results. XV. Gravitational lensing*, *A & A* **594** (2016) A15 [arXiv:1502.01591].
- [100] L. Anderson et al., *The clustering of galaxies in the SDSS-III Baryon Oscillation Spectroscopic Survey: Baryon Acoustic Oscillations in the Data Release 10 and 11 galaxy samples* *Monthly Notices of the Royal Astronomical Society* **441** (2014) 24 [arXiv:1312.4877].

⁴<https://github.com/ntveem/sterile-dm>

- [101] H. Gill-Marín et al., *The clustering of galaxies in the SDSS-III Baryon Oscillation Spectroscopic Survey: BAO measurement from the LOS-dependent power spectrum of DR12 BOSS galaxies* *Monthly Notices of the Royal Astronomical Society* **460** (2016) 4210 [arXiv:1509.06373].
- [102] S. Alam, et al., *The clustering of galaxies in the completed SDSS-III Baryon Oscillation Spectroscopic Survey: cosmological analysis of the DR12 galaxy sample*, *Monthly Notices of the Royal Astronomical Society* **470** (2017) 2617 [arXiv:1607.03155].
- [103] F. Beutler et al., *The 6dF Galaxy Survey: Baryon Acoustic Oscillations and the Local Hubble Constant*, *Monthly Notices of the Royal Astronomical Society* **416** (2011) 3017 [arXiv:1106.3366].
- [104] C. Heymans et al., *CFHTLenS: The Canada-France-Hawaii Telescope Lensing Survey*, *Monthly Notices of the Royal Astronomical Society* **427** (2012) 146 [arXiv:1210.0032].
- [105] M. J. Jee, J. A. Tyson, S. Hilbert et al., *Cosmic Shear Results from the Deep Lens Survey - II: Full Cosmological Parameter Constraints from Tomography*, *The Astrophysical Journal* **824** (2016) 77 [arXiv:1510.03962].
- [106] H. Hildebrandt et al., *KiDS-450: Cosmological parameter constraints from tomographic weak gravitational lensing*, *Monthly Notices of the Royal Astronomical Society* **465** (2017) 1454 [arXiv:1606.05338].
- [107] DES Collaboration, *Dark Energy Survey Year 1 Results: Cosmological Constraints from Galaxy Clustering and Weak Lensing*, (2017) [arXiv:1708.01530].
- [108] M. A. Troxel, et al., *Dark Energy Survey Year 1 Results: Cosmological Constraints from Cosmic Shear*, *Phys. Rev. D* **98** (2018) 043528 [arXiv:1708.01538].
- [109] Z. Hou, R. Keisler, L. Knox, M. Millea, and C. Reichardt, *How massless neutrinos affect the cosmic microwave background damping tail*, *Phys. Rev. D* **87** (2013) 083008 [arXiv:1104.2333].
- [110] A. Boyarsky, J. Lesgourgues, O. Ruchayskiy, and M. Viel, *Lyman- α constraints on warm and on warm-plus-cold dark matter models*, *JCAP* **0905** (2009) 012 [arXiv:0812.0010].
- [111] K. Abazajian, *Production and evolution of perturbations of sterile neutrino dark matter*, *Phys. Rev. D* **73** (2006) 063506 [arXiv:astro-ph/0511630].
- [112] A. Lewis, A. Challinor, *Weak gravitational lensing of the CMB*, *Phys. Rep.* **429** (2006) 1 [arXiv:astro-ph/0601594].
- [113] Planck Collaboration, Ade, P. A. R., Aghanim, N., et al., *Planck 2015 results XV. Gravitational lensing*, *Astronomy & Astrophysics* **594** (2016) A15 [arXiv:1502.01591].
- [114] K. N. Abazajian, K. Arnold, J. Austermann et al., *Neutrino physics from the cosmic microwave background and large scale structure*, *Astropart. Phys.* **63** (2015) 66 [arXiv:1309.5383].
- [115] E. Grohs, G.M. Fuller, C.T. Kishimoto and M.W. Paris, *Probing neutrino physics with a self-consistent treatment of the weak decoupling, nucleosynthesis and photon decoupling epochs*, *JCAP* **05** (2015) 017 [arXiv:1502.02718].
- [116] W. J. Percival, W. Sutherland, J. A. Peacock et al., *Parameter constraints for flat cosmologies from cosmic microwave background and 2dFGRS power spectra*, *Monthly Notices of the Royal Astronomical Society* **337** (2002) 1068 [astro-ph/0206256].
- [117] C. Howlett, A. Lewis, A. Hall, A. Challinor, *CMB power spectrum parameter degeneracies in the era of precision cosmology*, *JCAP* **1204** (2012) 027 [arXiv:1201.3654].
- [118] Planck Collaboration XXIV, *Planck 2015 results. XXIV. Cosmology from Sunyaev-Zeldovich cluster counts*, *A&A* **594** (2016) A24 [arXiv:1502.01597].
- [119] A. G. Riess, L. Macri, S. Casertano, et al., *A 3 % Solution: Determination of the Hubble*

Constant with the Hubble Space Telescope and Wide Field Camera3, The Astrophysical Journal **730** (2011) 119 [arXiv:1103.2976].